



UNIVERSIDAD NACIONAL AUTÓNOMA
DE MÉXICO

FACULTAD DE CIENCIAS

Quantitative biology assisted by automated
microscopy to study multicellular aggregates
of *Dictyostelium discoideum*

T E S I S

QUE PARA OBTENER EL TÍTULO DE:

Licenciado en Física

PRESENTA:

Sebastián González Tirado



TUTORES

Dra. Gertrudis Hortensia González Gómez
Dr. Christian Westendorf



Universidad Nacional
Autónoma de México

Dirección General de Bibliotecas de la UNAM

Biblioteca Central



UNAM – Dirección General de Bibliotecas
Tesis Digitales
Restricciones de uso

DERECHOS RESERVADOS ©
PROHIBIDA SU REPRODUCCIÓN TOTAL O PARCIAL

Todo el material contenido en esta tesis esta protegido por la Ley Federal del Derecho de Autor (LFDA) de los Estados Unidos Mexicanos (México).

El uso de imágenes, fragmentos de videos, y demás material que sea objeto de protección de los derechos de autor, será exclusivamente para fines educativos e informativos y deberá citar la fuente donde la obtuvo mencionando el autor o autores. Cualquier uso distinto como el lucro, reproducción, edición o modificación, será perseguido y sancionado por el respectivo titular de los Derechos de Autor.

1. Datos del alumno

González
Tirado
Sebastián
56 59 31 38
Universidad Nacional Autónoma de México
Facultad de Ciencias
Física
310010384

2. Datos del tutor

Dra
Gertrudis Hortensia
González
Gómez

Dr
Christian
Westendorf

3. Datos del sinodal 1

Dr
Enrique Salvador
Buzo
Córdova

4. Datos del sinodal 2

Dr
Gabriel Isaac
Corkidi
Blanco

5. Datos del sinodal 3

Dr
Roberto Carlos
Muñoz
Garay

6. Datos del sinodal 4

Jaime Arturo
Pimentel
Cabrera

7. Datos del trabajo escrito

Quantitative biology assisted by automated microscopy to study multicellular aggregates of *Dictyostelium discoideum*

60 p

2019

First of all I would like to thank Dr. Christian Westendorf for all the knowledge and expertise shed, his passion for science was the best piece of wisdom that I learned during the realisation of this work. I would also like to thank Dr. Gertrudis Hortensia González Gómez for all her support, comments, assistance, and willingness to be my tutor. Final thanks to Dr. Enrique Salvador Buzo Córdova, Dr. Gabriel Isaac Corkidi Blanco, Dr. Roberto Carlos Muñoz Garay, and Dr. Jaime Arturo Pimentel Cabrera for kindly accepting my invitation to be part of my examination jury.

Contents

Contact	i
Acknowledgments	i
Abstract	xi
1 Introduction	1
1.1 <i>Dictyostelium discoideum</i>	1
1.1.1 Chemotactic response	3
1.1.2 cAMP waves	4
1.2 Phase contrast microscopy	4
1.3 Fluorescence microscopy	4
1.4 Image processing	6
1.4.1 K-clustering	7
1.4.2 Spatial convolution	9
1.4.3 Filters	10
2 Aims of thesis and objectives	11
2.1 Aims	11
2.2 Objectives	11
3 Material and Methods	13
3.1 Cell culture	13
3.1.1 Cell harvesting	13
3.1.2 Labeling with Cell Tracker TM	14
3.2 Experimental set-up	14
3.3 Image processing	15
3.3.1 Correlation and merging	16
3.3.2 Image binarization	17
3.3.3 Filtering and centroid calculation	19
3.3.4 Positions over time	20
3.4 Aggregation statistics	20
3.5 cAMP waves	20

4	Results	23
4.1	Time evolution	24
4.2	Chemotactic angle	26
4.3	Velocity	28
4.4	Passing waves	28
5	Conclusions	31
A	Analysis list	39
B	Assembly	41
C	Binarization	47
D	Obtain Tracks	51
E	Velocity and Angle Calculation	55

List of Figures

1.1	<i>D. discoideum</i> morphogenesis	2
1.2	Phase contrast microscope optical train	5
1.3	Jablonski diagram	6
1.4	Image processing motivation	7
1.5	General procedure for k-means clustering	8
1.6	Gaussian filtering	10
3.1	Microscope arrangement	15
3.2	Phase contrast images from same set	16
3.3	Merged frame	17
3.4	Pixel intensity histogram	18
3.5	Frame image before and after binarization	19
3.6	Extraction of physical values	21
3.7	cAMP gradient estimation	21
4.1	Individual trajectories towards aggregation center	23
4.2	Time evolution surface plots	25
4.3	AgC problematic	26
4.4	Time evolution of chemotactic angle for initial times	27
4.5	Time evolution of chemotactic angle at aggregation	27
4.6	Velocities time evolution at initial stages	28
4.7	Velocities time evolution at aggregation	29
4.8	Velocity of cells vs distance from aggregation center	30

List of Abbreviations

AgC	Aggregation center
cAMP	3'-5' cyclic adenosine monophosphate
ACA	Adenylate cyclase
<i>D. discoideum</i>	<i>Dictyostelium dicoideum</i>
CA	Chemotactic angle
PB	Phosphate buffer
PCM	Phase contrast microscopy
PTEN	Phosphatase and tensin homolog

Abstract

There are biological systems which show spontaneous pattern formation occurring at nonequilibrium conditions. One example is the cell migration patterns and motion observed during the life cycle of the social amoeba *Dictyostelium discoideum*, which is an unicellular amoeba that enters into a multicellular developmental program when facing conditions of low or no nutrients, making it of great interest for research in different branches of human knowledge. The gathering of cells into a multicellular complex is mediated, among other factors, by the chemotactic response to 3' -5' cyclic adenosine monophosphate (cAMP), which is synthesised, recognized, and relayed by *D. discoideum*. This is a complex phenomena, far from equilibrium and of great interest to study with reliable tools that can provide exact measurements.

This thesis concerns with the implementation of an automated stage to study the aggregation process of *D. discoideum* through microscopies techniques that included phase contrast and epifluorescence. Automated microscopy was used to increase the observable region of interest and thus available statistics of different parameters like the velocity and chemotactic response of the cells while preserving a spatial high resolution.

Image processing was used to segment and analyze the data, creating a sequence of algorithms that were able to follow the paths of different cells during the aggregation stage and quantify the velocity and angular distribution with respect to the aggregation center. The goal was to develop tools to extract value parameters as the concentration and signal shape of cAMP waves in an attempt to adapt the obtained results to an already established model for stochastic description of *D. discoideum*. This tools try to solve some problems found in existing programs for cell tracking and a comparison between them and the developed methods in this work are discussed. A quantification of these properties was succesfully done while the stochastic model adapted to this system is still missing.

An algorithm workflow was written so it can be used for similar problems by the scientific community. This algorithm workflow was written in Matlab

for several reasons: the program's computational power to process data in parallel looping, its extensive functions library which provides versatility for plotting and other tasks, and the possibility of tracking cells whose fluorescent signal can be lost.

Introduction

Collective cell migration is often described as a process where groups of cells move to new regions in order to perform specific biological tasks and it is a key component in the development of living organisms. It plays a significant role in organogenesis, immune reactions (Negulescu et al. (1996)), tumor metastasis (Condeelis and Segall (2003)), and the development of the nervous system (O'Rourke et al. (1992)). This movement is controlled by chemotaxis, which is defined as the response of a cell towards or away from a chemical stimulus. *Dictyostelium discoideum* is a social amoeba of great interest as a model organism for the study of collective motion, cell motility, chemotactic response, phagocytosis, cell adhesion, and pattern formation, among many other applications (Kessin (2001)). This is explained by the interesting life cycle of *D. discoideum* where, upon starving conditions, relinquishes its amoeboid state to form a multicellular organism within its developmental life cycle (see Figure 1.1).

1.1 *Dictyostelium discoideum*

Amoebas are micro-organisms that belong to the **Protista** kingdom of the **Eukaryota** domain, which is composed of unicellular living beings that can live separated from each other or in a colonial-way stacked together in large bodies but without forming tissues or complex multicellular bodies. They have a similar structure to that of animal cells and have 10-100 times the diameter of bacterias Jeon (2012).

D. discoideum is an amoeba that lives in forest soil as a single cell, feeding on bacteria and reproducing until starving conditions become present and halt its life cycle. The amoeba is able to take immediate action upon this nutrient

shortage by induction of genes in order to stop metabolic processes like cell growth and start the synthesis of a signal molecule that guides itself the formation of multicellular aggregates. During this process, cells stream toward a central domain referred to as the aggregation center. This results in the formation of a mound which further grows to form a finger. If the extended finger falls, it will form a phototactic migration slug, a stage that does not occur always. At the final stages the finger or slug give rise to a fruiting body supporting a spore head containing spores. These spores have a higher tolerance to different environmental conditions than the amoeba and can germinate into the latter ones, completing the life cycle [Kessin \(2001\)](#). A short sketch showing some stages of *D. discoideum* morphogenesis is given in [Figure 1.1](#).

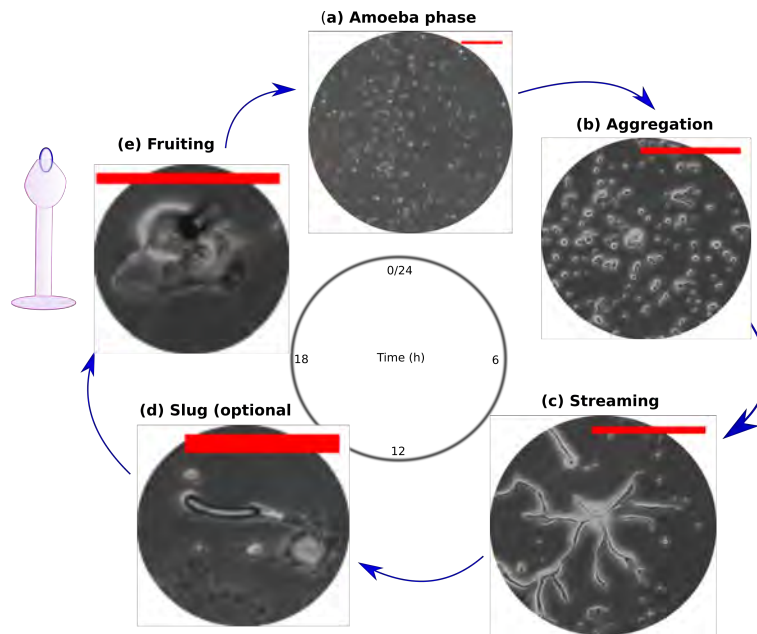


Figure 1.1: Phase contrast images of selected stages from *D. discoideum* social morphogenesis. The amoeba phase is shown in (a), where the signaling of cAMP is not still present. (b) shows the first stages of aggregation with directed movement. (c) is the streaming phase where cells can move along each other together. (d) shows the formation of a slug, which does not occur always and the life cycle can progress directly to the fruiting body in (e), with a drawing to clarify the microscope image. Scale bars, 200 μm in (a), (b), (c), and 50 μm in (d), (e).

The main chemical mediator that orchestrates the formation of aggregates and consecutive multicellular stages is 3',5'-cyclic monophosphate (cAMP). This is produced by cells in some areas until a high concentration is reached and cells excite themselves and neighbours to start producing and secreting more cAMP, in an autocrine signal ([Gerisch et al. \(1979\)](#), [Tomchik and Devreotes \(1981\)](#)). This molecule has extracellular and intracellular functions: extra-

cellularly as a ligand for G-protein-coupled receptors, while intracellularly it activates cAMP-dependent protein kinase (Chisholm and Firtel (2004)). The life cycle can be studied by removing nutrient sources and placing cells on agar as a layer, where they start to synthesize and secrete cAMP three to four hours after undernourished conditions (Fey et al. (2007)). At the aggregation stage *D. discoideum* can move as fast as 10-15 $\mu\text{m}/\text{min}$ (Varnum and Soll (1984)). They perceive increasing and decreasing gradients of cAMP that can differ between the front and back parts of the cell by discrepancies of only a 2% (Devreotes et al. (1979)).

1.1.1 Chemotactic response

The directed motion towards or away from a chemical stimulus is known as chemotaxis. The chemotactic response of *D. discoideum* to the cAMP molecule mediates the aggregation stage of the developmental life cycle. Three main steps describe the whole chemotactic process: sensing, polarization, and migration.

On the first step the cells sense and recognize gradients of cAMP through transmembrane receptors (cAR1), getting to know the direction with higher concentration of cAMP. These receptor proteins are also G-protein coupled receptors and are in charge of switching on the signal to activate a downstream cascade of chemical processes through the cell. This cascade is turned on as the cAMP binds to its receptor, which then dissociates the G-protein and therefore activates different GTPases. On the other side of the cell, an opposite reaction is mediated by the phosphatase PTEN, which translates the outer cAMP gradient into an internal gradient.

After the directional sensing the cell polarizes and adopts an elongated shape prior to migration. A stable leading edge forms in the direction with steeper cAMP gradient, while the rear of the cell forms at the side with lower concentration. A complete picture of the chemotactic response is still missing because different signaling mechanisms have been discovered.

An increase in actin filaments at the front creates a protrusion. It is still not clear whether the cell movement is mediated through the inner gradient, as previously explained, or if it is directed through a bias created by the chemoattractant. In the second approach, called pseudopod-centered, the chemoattractant creates a weight in the pseudopod formation and its lifetime, making it shorter for the rear and causing a faster retraction of that part (Andrew and Insall (2007)). The rear contracts thanks to myosin motors located on the actin network, consisting of a crosslinked network of actin fibers.

1.1.2 cAMP waves

The production, secretion and signal relay of cAMP by *D. discoideum* cells forms complex patterns with far from linear behaviour. The dynamics of the cAMP waves can be calculated from optical density techniques during the aggregation stage. It has been reported that waves propagate fast at the initial stages ($600 \mu\text{m min}^{-1}$) with a low frequency (once every 6-8 minutes [Rietdorf et al. \(1996\)](#)). Binding of cAMP to its specific receptor triggers two competing processes: an earlier activation of adenylate cyclase (ACA) and synthesis of cAMP, and a slow adaptation that results in an inhibition of ACA [Fisher \(1991\)](#). The cells adapt and stop producing cAMP because of autocatalytic feedback produced by the binding of cAMP secreted by the same cell (inhibition by product). As the cells secrete cAMP phosphodiesterase that degrades cAMP the concentration of cAMP will fall, as adaptation is present. The De-adaptation occurs by a fall of extracellular cAMP concentration. This adaptative process is the one responsible for the cAMP waves propagating outwards as cells that just relayed the signal are refractory to stimulation. The cells respond to the steeper gradients of cAMP and stop moving as the concentration decreases, which prevents that they follow the wave once the signal has passed [Futrelle \(1982\)](#). All this chemotactic response results on the periodic movement of the cells toward the aggregation center because of the outward propagating waves.

1.2 Phase contrast microscopy

The human eye is uniquely sensitive to differences in amplitude of light (distinguished as brightness) and wavelength (color), while differences in phase are not distinguishable to it. Many objects can cause changes in the phase of incident light by modifying the optical path length, either by differences in thickness or refractive index. The PCM is a technique that phase shifts the zero-order beam (visualized as the central maximum in a diffraction pattern) in the microscope such that a contrast in intensity is formed as the shifted beam recombines with the following orders. To achieve this, an annulus condenser is used to impact only the zero-order of the illumination light with a phase shift induced later on by the phase plate as shown in [Figure 1.2](#).

1.3 Fluorescence microscopy

Fluorescence and phosphorescence are two physical phenomena in which an organic or inorganic specimen emits radiation after being excited with light of a specific wavelength, usually of higher energy (lower frequency) than the

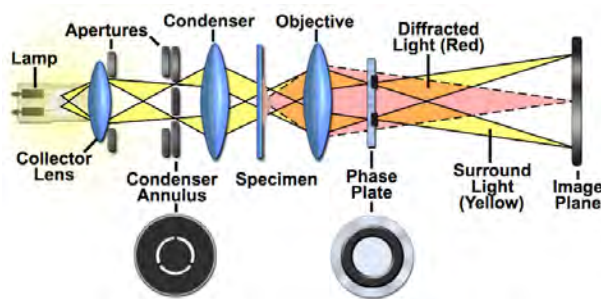


Figure 1.2: Phase contrast microscope optical train. The light coming from the collector lens goes through the condenser annulus to let the zero-order beam pass. The light is further diffracted in the specimen by differences in thickness and refractive index (n). The phase plate makes a shift in phase which can be then captured by a camera. Image taken from <http://www.microscopyu.com>, Nikon.

emitted. The difference between excitation and emission wavelengths is known as the Stokes shift and it was named after the british scientist who in 1852 saw the emission of red light in the mineral flourspar after exciting the compound with ultraviolet light. The absorption and emission of light occur almost simultaneously within a time range of nanoseconds. When the persistence of the emitted light is longer, then the phenomenon is referred to as phosphorescence. (Lichtman and Conchello (2005)). Fluorophores are molecules that exhibit this behaviour.

From the physical point of view, fluorescence occurs when excitation photons transfer energy to the molecule making changes in electronic, vibrational and rotational states. This process originates transitions of the electrons in the outermost orbital from a ground state to an excited state. Molecules with some degree of conjugated double bonds can fluoresce with smaller Stokes shift because of the electron distribution on them. These compounds have ring structures very often (aromatic molecules) with pi bonds that have a large area in which the outer electrons are.

Jablonski diagrams are used to depict the energy states of a fluorophore. Figure 1.3 shows a Jablonski diagram with the energy states and possible pathways during the absorption of light. Electrons are excited by light and climb to higher energy levels. Electrons spin, and hence the total angular momentum, can also change during this process. The total angular momentum is given by $2S + 1$, where S is the total spin. For singlet states with antiparallel spins of $1/2$ and $-1/2$ this is 1, and when an intersystem crossing occurs then the excited electron also changes its spin and hence the total angular momentum will be 3, triplet state. Because of the exclusion principle of Pauli the excited electron on the triplet state can not go back to the same ground state until it changes its spin again. This reason explains why phosphorescence has a higher lifetime than fluorescence.

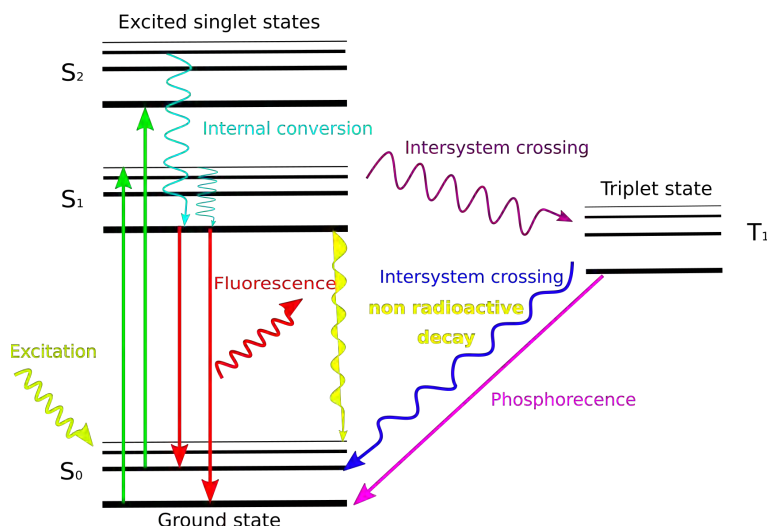


Figure 1.3: Jablonski diagram with the energy states of a molecule and the possible processes that can occur. Fluorescence occurs when the singlet state emits the energy previously transferred in the form of light. Intersystem crossing changes an excited electron spin and generates a triplet state which phosphoresces when the electron falls down to the ground state.

The main approach in fluorescence microscopy is to excite with light fluorophores, who have ligands that can attach to specific molecules or compartments in the cells, and observe the emitted light produced by the transition of electrons to a lower state.

1.4 Image processing

Like all the human senses the vision is highly developed and because of this reason images play an important role in perception. Although we can only see in a short range of the electromagnetic spectrum, the development of machines has abled the possibility to see beyond our capabilities, from X-rays, to ultrasound and microwaves. Digital image processing has become an important research area and a lot of work in this field is being made to address problems like image coding, image restoration, 3D image processing, feature extraction and analysis, moving object detection, and face recognition [Jensen and Lulla \(1987\)](#). In biophysics it has been widely used to make quantitative studies of cell migration.

A digital image can be defined mathematically as a function $f(x, y)$ with the domain in a two dimensional space. Each coordinate of (x, y) represents the location of a point and the amplitude f defines the intensity or gray level at that position. All of these values are discrete quantities and are referred to

as *pixels* (Gonzalez et al. (2002)).

The motivation for using image processing is to extract the data of interest for studying *D. discoideum's* life cycle. The required information is comprised of the distinction from individual cells between them and from background. This is a challenging task because of the large number of cells in the visual area and the possibility of merging between them (when two or more cells stack together), but it is a crucial step in order to correctly quantify different parameters as the motion, velocities and directionality. Figure 1.4 shows two different observations with a time gap of 2 hours between them; how can we describe the transition in time of all the elements from Figure 1.4(a) to 1.4(b)? The next sections will discuss how the location of single cells was assigned and the methods used for it.

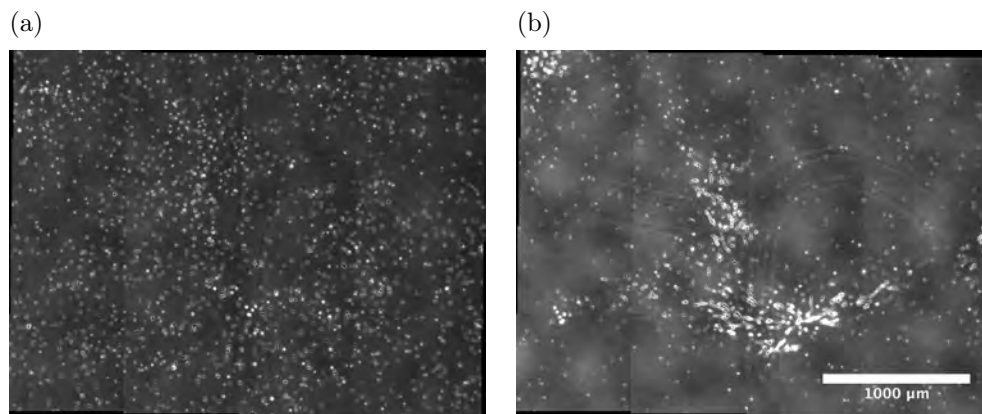


Figure 1.4: *D. discoideum* at different stages of its life cycle. (a) shows a set of cells after 1 hour of starving conditions while in (b) the same population was observed after 2 hours.

1.4.1 K-clustering

Clustering is a technique used to assign a cluster or center from the set $\mathcal{C} = c_1, c_2, \dots, c_k$ to each data point from a set $\mathcal{P} = x_1, x_2, \dots, x_n$. The assignment is done by finding how similar are the data points to each of the cluster centers through the definition of some metric between both sets. A very common metric used is the typical euclidean distance and with this the assignment is performed by minimizing:

$$\sum_{i=1}^k \sum_{x \in \mathcal{P}} \|x - c_i\|^2. \quad (1.1)$$

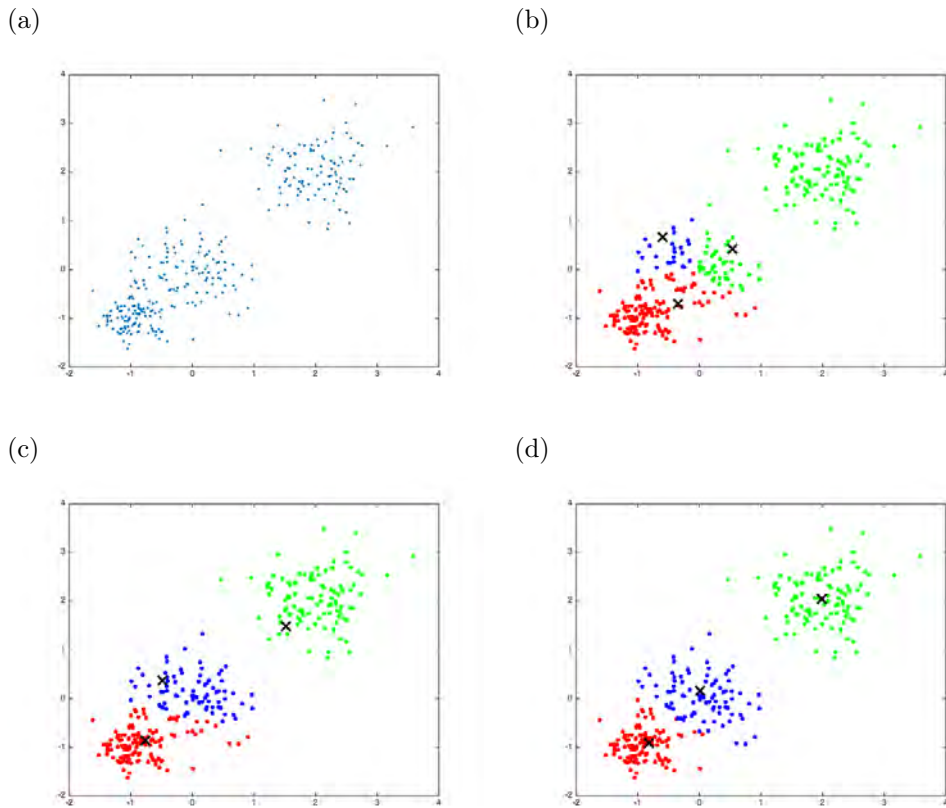


Figure 1.5: General procedure for k-means clustering. (a) shows random generated data with three different weights. Cluster centers are initialized randomly in (b), assigning each data point to its closest center as shown with different colors. (c) New centers are defined by averaging the obtained data points from each cluster and making a new assignment. (d) Loop is run until a minimum of the metric sum between data points and cluster centers is found.

The position of the centers is randomly initialized and changed until a minimum is achieved. At each loop in the algorithm a new center is defined by taking the average of the points already assigned to it and running the whole process of assignment again. The algorithm can proceed as marked by the following points (Spath (1985)):

- Select k initial clusters randomly.
- Compute the distance given by a specific metric from each data point to each cluster.
- Update the batch: reassign points to their nearest cluster centroid by

iterations and recalculating cluster centroids.

- Obtain k new cluster locations by the averages obtained.
- Repeat until cluster assignments stop changing, which means that the minimum was reached, or stop after a certain maximum value of iterations is reached.

This technique is used in image segmentation to separate different objects and be able to distinguish a specific collection or part of interest from a sample. The data point set and cluster centers set can be defined by the pixel intensity values, obtaining thresholds for the different objects. Clustering of cells was efficient because of the microscopy techniques used. There is a big difference in the intensity of cells and background both in phase contrast and fluorescence, which allows an optimal performance of the algorithm. Interestingly, mammals use a similar mechanism called lateral inhibition where a neuron can reduce the activity of its neighbours under some stimuli, increasing the contrast in stimulation [Ungerer and Schmid \(2013\)](#). K-means clustering was used here to differentiate pixels corresponding to cells and those belonging to the background.

1.4.2 Spatial convolution

Convolution is a fundamental mathematical operation used for many image processing operations like filtering. It consists of scanning an input image with some specified kernel (given as a matrix of smaller size) which multiplies and adds the values of the input submatrix at which the kernel is superimposing to give a new image.

The kernel can have different values and this also defines the purpose it has. The Gaussian convolution is used to remove detail and noise with the kernel being represented by an origin-centered 2D Gaussian function $g(x, y) = \frac{1}{2\pi\sigma^2} e^{-\frac{x^2+y^2}{2\sigma^2}}$. This kernel gives more weight at the central pixels and less to the neighbors; the farther away the neighbours, the smaller the weight. [Figure 1.6](#) represents the effect of this kernel for a standard deviation of $\sigma = 3$.

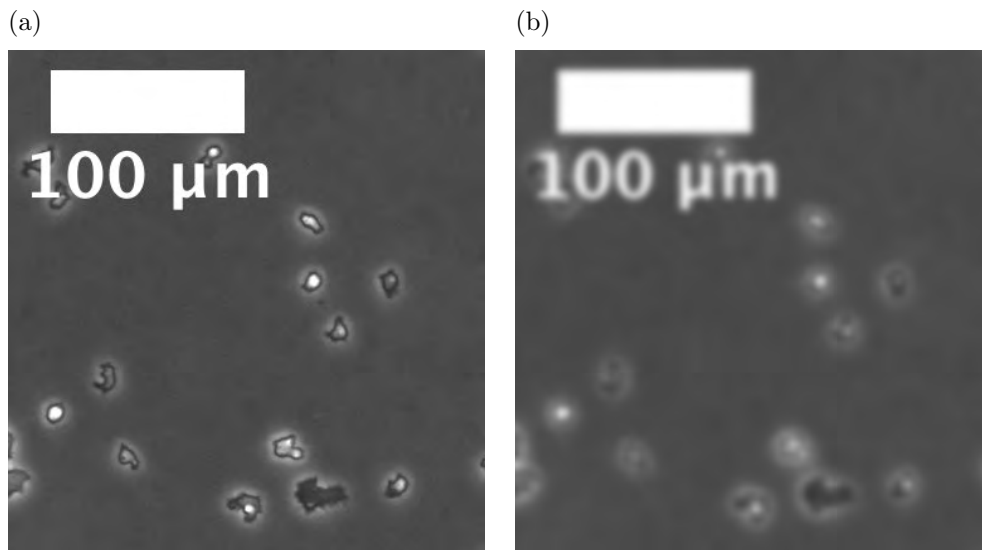


Figure 1.6: Effect of Gaussian filter with standard deviation of $\sigma = 3$. (a) Input image before convolution. (b) filtered image with blurry effect.

1.4.3 Filters

A mask or kernel in a convolution is the same concept as that of a filter in the frequency domain. A blurring kernel, like the Gaussian described before, reduces the edge content of an image (Figure 1.6) and it corresponds to a low pass filter. A mask that enhances edges, on the other hand, corresponds to a high pass filter.

Aims of thesis and objectives

2.1 Aims

- The automatization process can help to reveal more accurate value parameters on the aggregation stage of the biological model organism *Dictyostelium discoideum*. This high accuracy will be obtained from scanning broader areas while maintaining a high resolution.
- It is possible to write an algorithm pipeline that can track cell trajectories even when photobleaching occurs.
- Chemotactic response and parameter values of *Dictyostelium discoideum* life cycle can be extracted with computational tools.

2.2 Objectives

- Write a complete pipeline of algorithms that will merge the data obtained from the frames of the automated stage, process the images to distinguish the position of individual elements, track the displacements in time and quantify the aggregation stage of *Dictyostelium discoideum* morphogenesis.
- Get an estimation of values like the concentration and variation of cAMP during the aggregation stage using a tracking algorithm that can provide high quality data from the processed images.
- Study distinct features of the *D. discoideum* aggregation stage like the velocity, chemotactic response, pattern formation, and wave signaling.

- Obtain values of cAMP concentration and see the relationship of these with cell movement.
- Compare the algorithm pipeline with other available tools for image analysis and cell tracking.

Material and Methods

Experiments consisted in the observation of harvested cells moving and thereby aggregating in agar inside glass bottom dishes. The starting time was around one hour after starving conditions and it lasted approximately 20 hours. The PCM and fluorescence microscopy techniques collected the data to 50 MHz and with a time gap of 1.014 s between subsequent images. The automated stage moved such that 16 or 25 adjacent images for each microscopy channel were obtained. PCM was used to achieve high contrast between the cells membrane and background due to the transparency of cells while fluorescence was used to track the displacements of a minor population in order to reduce the combinatoric task of the algorithm.

3.1 Cell culture

The culture of *Dictyostelium discoideum* was maintained in HL5 medium at 22 °C in a Petri dish until its harvesting for experiments and before it was stored at -80 °C either as cells or spores for an extended period. The cells were frozen in HL-5 medium (14 g/L peptone, 7 g/L yeast extract, 13.5 g/L glucose, 0.5 g/L KH₂PO₄, 0.5 g/L Na₂HPO₄ from Formedium) with an additional 20% Dimethyl sulfoxid (DMSO, Calbiochem) and 40% Fetal calf serum (FCS, Invitrogen) and spores were frozen in liquid nitrogen.

3.1.1 Cell harvesting

The following protocol was carried out prior to all experiments:

1. Removal of medium and floating cells from Petri dishes.

2. Mixed the cells attached to the bottom of two Petri dishes with 10 ml of phosphate buffer (PB).
3. The cell suspension was centrifuged at 4°C to 1000 rpm for 3 minutes (first wash).
4. For two consecutive runs the supernatant was again removed leaving only a pellet of cells at the bottom of the tube and repeating the last step. 10 ml of PB were used for the final cellular suspension.
5. 300 μ l were distributed over MatekTM glass bottom dishes with a layer of 1.2% agar. The cells were distributed with vertical and horizontal plane movements and left with the lift open for 5-10 minutes to let the excess of PB evaporate.

3.1.2 Labeling with Cell TrackerTM

Cell Tracker Green CMFDA Cat. C7025 and Cell Tracker Red CMTPX Cat. C34552 (Thermo Fischer Scientific, Massachusetts, USA) were used to stain approximately 2.5% of the total population with a specific fluorescent label. The dyes bind to the microtubuli inside the cells. After harvesting the cells, two or three tubes of 1 ml were filled with the obtained cell suspension (2 for one fluorescent stain and 3 for two stains). The cells to be stained were mixed with 2 μ l of 10mM Cell TrackerTM Red and Green, which have an absorption maxima of 577, 492 nm, and excitation maxima of 602 and 517 nm, respectively. All tubes were shaken for 45 minutes at 22 °C and 300 rpm. 950 μ l of the control (unstained) cells were mixed with 25 or 50 μ l of the stained cells (always 25 μ l for each label). Cells stained with Cell Tracker were kept in dark to prevent photodamage.

3.2 Experimental set-up

Control of microscope and stage through the Micro-Manager open software. Sets of PC and fluorescent (red dye) images were recorded for 20 hours with the automated stage to 0.16 Hz frequency (1 minute) between subsequent sets using an Olympus IX81 inverted microscope (3.1) and 10X LCPLN (Olympus) objective with 0.25 numerical aperture. Each set consisted of 16 or 25 frames (4 rows and 4 columns for the 16 frames sets and 5 rows and 5 columns for the other case) and was recorded with both PCM and fluorescence microscopy and a 10% overlap between neighbouring images. The 10% overlap was done such that the images could be aligned and overlaid using cross-correlation.

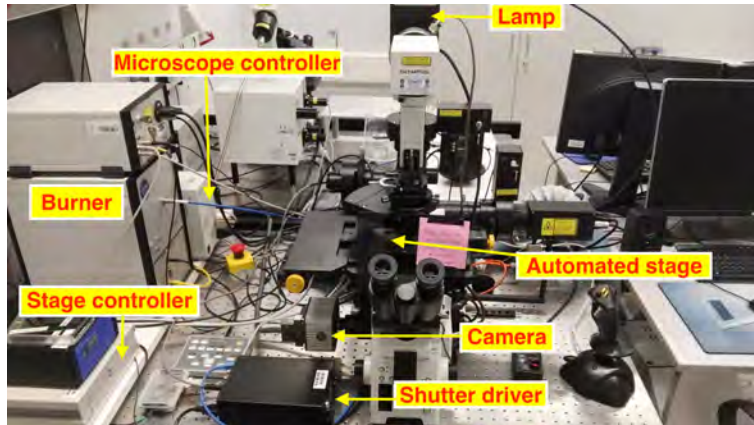


Figure 3.1: Microscope arrangement with an automated stage mounted on an inverted Olympus IX81 microscope. The Burner is the source of a high-intensity light (mercury arc lamp). The stage controller operates the speed and movement of the stage and the shutter driver is used to create digital images of the observed specimen.

Each PC and fluorescent image was captured using a Hamamatsu CCD camera with an exposure time of 400 ms and a spatial resolution of 1344×1024 pixels (1 pixel = $0.6465 \mu\text{m}$). The time gap between subsequent frames of one set was of 1.098 s, with the automated stage movement as the one shown in Figure 3.2. The microscope and automated stage were controlled through a Python GUI connected to the core of a Micro Manager open source software program developed by the UCSF (Edelstein et al. (2014)).

3.3 Image processing

This section presents the workflow of algorithms used to segment, denoise, filter, and detect the data such that the displacements of cells could be tracked and analyzed. First, images were recorded with a 10% overlap such that they could be aligned and overlaid by subsequent cross correlation. Afterwards a binarization of the images was done using k-means clustering to recognize cells from background signals. As only the movement of single cells was of interest, further processing was done to detect circular shapes between a size interval, thus avoiding the measurement of groups of membrane attached organisms. The tracks of cells were reconstructed from the merged-binarized images by finding the centroids of all positions from a determined set of frames and minimizing the mean square displacement of all the possible trajectories between centroids of subsequent frames in a given set. Angles and velocities of the tracks were calculated. The main steps are the following:

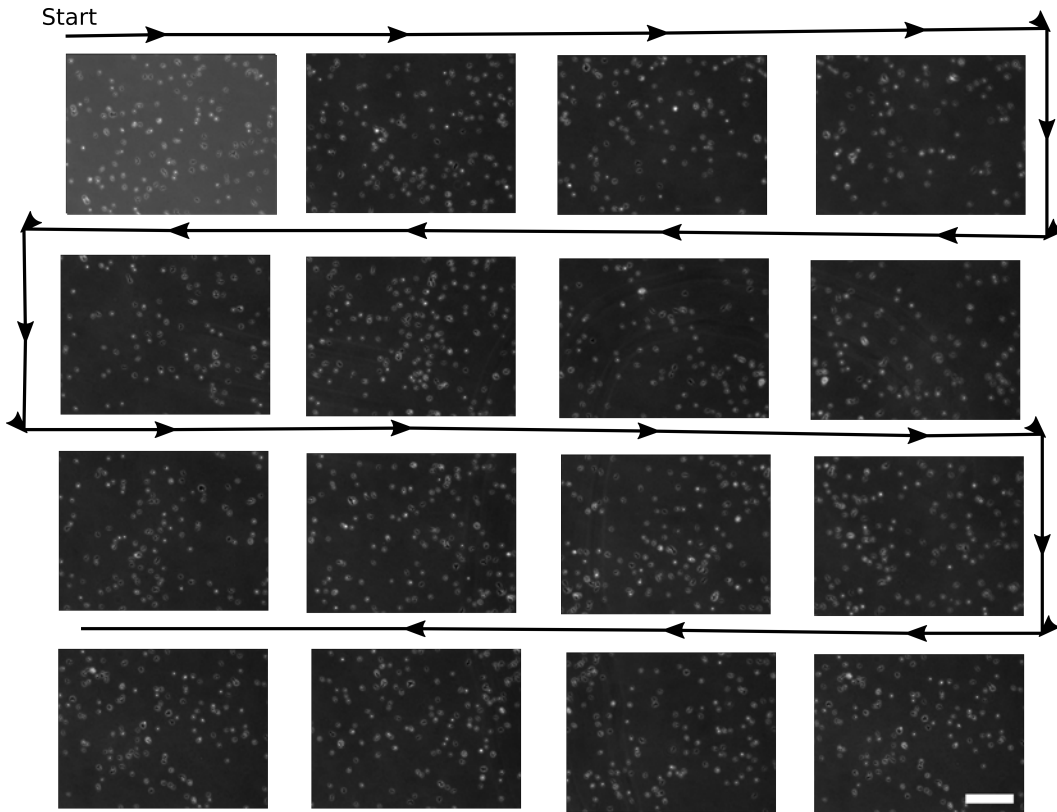


Figure 3.2: Single phase contrast images showing the automated stage movement. There is a 10% overlay between subsequent images. The time interval between each adjacent position is of 1.014 s. Scale bar equals 200 μm .

- Assembly.
- Binarization.
- Cell tracking.
- Angle and velocity calculation.

3.3.1 Correlation and merging

In order to merge the individual images obtained from the automated stage (see fig. 3.2) into a whole frame (fig. 3.3), a correlation algorithm was implemented to localize the exact position of the offset area. This last one made use of the built-in 'normxcorr2' function of MATLAB to calculate the correlation between consecutive images. The cross-correlation was calculated in the spatial domain, considering each image as a 2D function $f(x, y)$, the array of pixels and pixel intensity as the domain and codomain, respectively ((Lewis (1995), Haralick and Shapiro (1992))). The correlation coefficients were obtained by

precomputing running sums (means) and normalizing. This is represented with equation 3.1, where f is the image, t the template, and the evaluation over (u, v) is on the template region. Means are represented with upper hats.

$$\gamma(u, v) = \frac{\sum_{x,y} [f(x, y) - \bar{f}_{u,v}] [t(x - u, y - v) - \bar{t}]}{\left(\sum_{x,y} [f(x, y) - \bar{f}_{u,v}]^2 \sum_{x,y} [t(x - u, y - v) - \bar{t}]^2 \right)^{0.5}} \quad (3.1)$$

The maximum of this value will show the region where the maximum correlation was found. The alignment vectors obtained were used to align the respective frames of the fluorescent images. This method showed to have an error below 2% for the superposition of cells in adjacent frames.

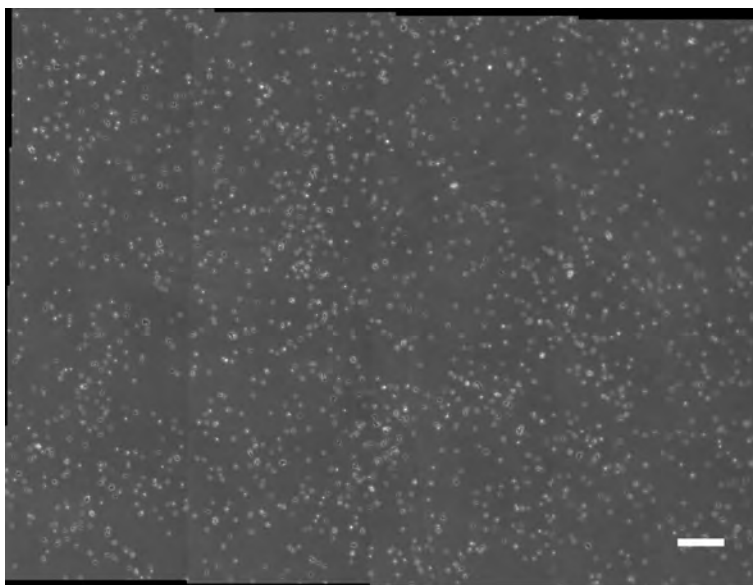


Figure 3.3: Combined frame created by aligning the individual frames from Figure 3.2 with the coordinates found with the maximum correlation between offset regions of subsequent images. Scale bar equals to 200 μm .

3.3.2 Image binarization

Data points of interest had to fulfill some requirements. The first one was to have a high pixel intensity value in order to discard noisy points presenting photobleaching or background signal. Rod-like shaped objects were also excluded to avoid the detection of bundles of cells.

A binarization of the *foreground* pixels (the cells) and the background was performed by doing k-means clustering of the pixel amplitude with the goal to determine whether a pixel belonged to the *background* set, or if it was member of the *foreground* set. Figure 3.4 shows the normalized pixel intensity histogram from (c) of Figure 3.5. A Gaussian shaped distribution is obtained for the pixel values from the background, while the *foreground* values can not be distinguished. Only objects with a bigger count of 10 connected pixels were classified as being part of the cells group. Cells had a size between 5 and 10 μm in diameter and this corresponds to groups of 10 to 50 pixels.

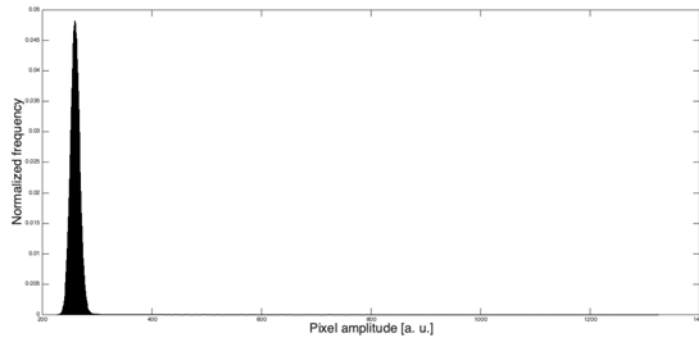


Figure 3.4: Pixel intensities normalized histogram. The values obtained were used for the k-means clustering algorithm to determine if a pixel belongs to a cell of interest or if it will be treated as background. The cluster centers for this example were: $C_1=259.51$ and $C_2=500.82$

A morphological disk structuring element was used to convolve with the cell clusters and achieve better defined borders and shapes. The pixels with no signal contained in these disk-shaped cells were changed for pixels that corresponded to cell signal. This was done to get completely connected clusters and take into account points within the cells where signal intensity was low and not detected as belonging to the cell.

Figure 3.5 shows images before and after the binarization. 3.5 (a) is the whole 4x4 merged analysed image and the result is shown in 3.5 (b). 3.5 (c) is a zoomed region of 3.5(a) with arrows showing objects that are not considered for the tracking analysis since they are not bright enough, do not have a circular shape or have a radius below .

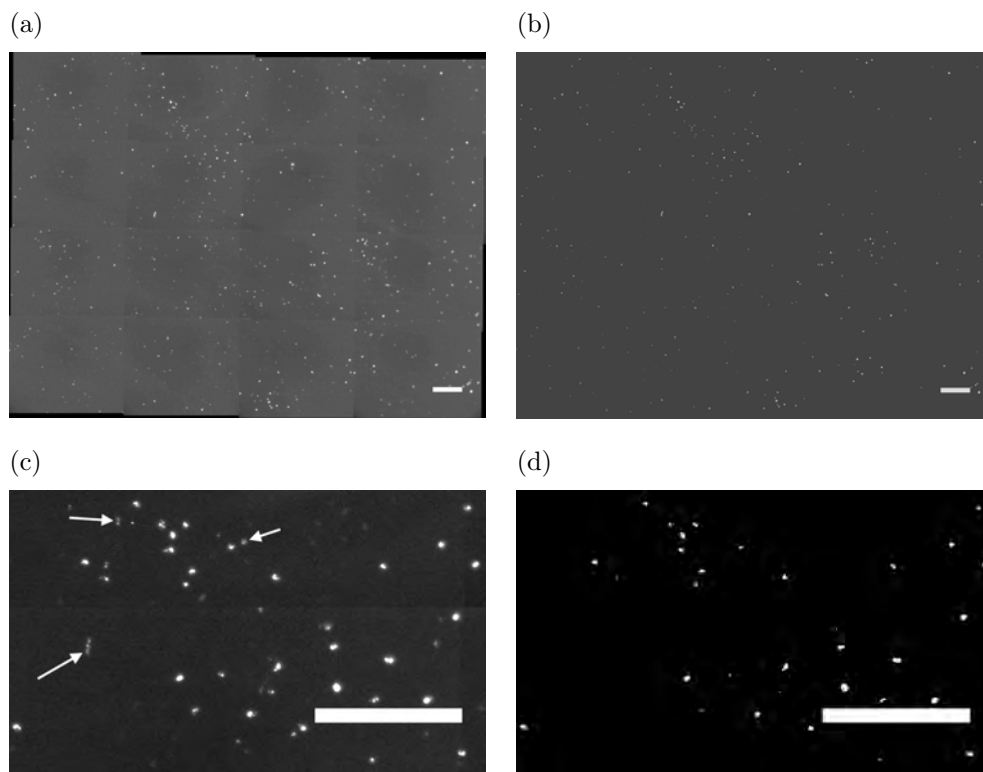


Figure 3.5: Input and output of image processing method where thresholding, dilation, erosion, and filling are applied. In (a) are the 4X4 aligned images prior to the process showing the result in (b). Detailed areas of (a) and (b) are shown in (c) and (d) respectively. Elongated, small, and dim objects as the ones shown by the arrows in (c) are not detected or discarded and thus not seen on the final binarized mask showing the same region in (d). Scale bars equal $200 \mu m$ in all images.

3.3.3 Filtering and centroid calculation

This section describes how the center of a cell is calculated to pixel level accuracy. The binarized images were smoothed using a real-space band pass filter from [Blair and Dufresne \(1997\)](#), which also suppresses long-wavelength image variations and retains objects information of a characteristic size. The band-pass is obtained by subtracting an image convolved with a boxcar kernel from an image convolved with a Gaussian kernel. The Gaussian filtering performs a lowpassed version of the original image, while the boxcar filtering sharpens the edges of objects and makes a highpass filter. This results in sharply peaked circular objects.

The local maxima were obtained in a two step process using algorithms developed by [Blair and Dufresne \(1997\)](#) and based on ideas from [Crocker and Grier \(1996\)](#). First, pixels above a specified threshold (which depends on brightness of objects) are extracted. The brightest pixel is found within

connected pixel clusters and an image with all this peaks is formed. To avoid the detection of peaks related to the same cell, a second search of local maxima is done for each peak within a specified kernel size given by the average cell size which was of 31 pixels (20 μm radius). The second step of the center localization corresponds to a sub-pixel accuracy calculation (Crocker and Grier (1996)).

3.3.4 Positions over time

The centroid calculation gave the approximate positions of cells with respect to time, the tracking of this array listing of scrambled coordinates works as following: having n positions of data points at time $t(i)$ and m positions at time $t(i+1)$, all the possible connections between points of successive times are calculated, choosing those which have the minimal total square displacement. A parameter of maximal dispersion is defined as the maximal number of time frames in which a particle can disappear and appear again (this was observed to happen across all observations). This can also penalize the weighting function by a factor of $max.disp^2$ in order to avoid identification of new points which correspond to previous trajectories.

3.4 Aggregation statistics

In order to quantify the way in which the cells responded to the signal from the AgC, a chemotactic angle, θ , was defined as the angle between the vector pointing to the aggregation center from the current cell position and the displacement vector after a time step, as depicted in Figure 3.6. The aggregation center was chosen by observations of the streaming phase, where a center of aggregation was possible to visualize.

3.5 cAMP waves

An indirect method to measure the cAMP concentration with respect to distance from aggregation center for different times was developed to show a possible application of the cell tracking and analysis. Figure 3.7 shows this idea pictorially. The velocity means of cells located in one of subsequent rings with center at the AgC were related to the concentration of cAMP, as cells can distinguish between cAMP values (Devreotes et al. (1979)).

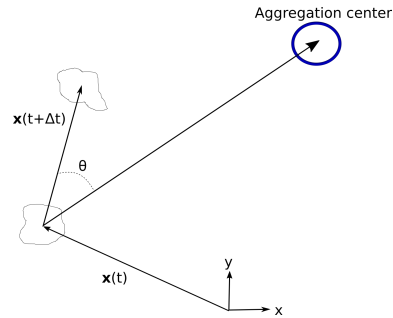


Figure 3.6: Coordinate system showing the meaning of the different quantities to be calculated. Aggregation center was chosen at the end of the streaming phase when a clear circular shaped organism was formed by the aggregation. The angle θ was defined as the chemotactic angle and it is defined as the difference of angle between a straight walk to the aggregation center and the next step made by the cell.

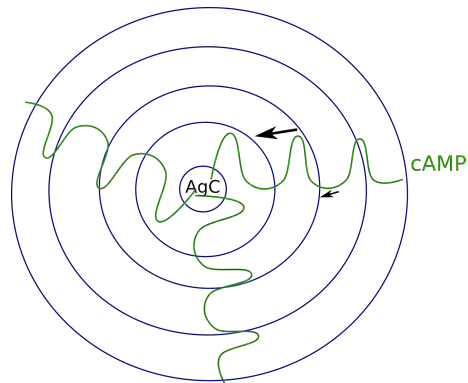


Figure 3.7: Method on which cAMP concentration profile was estimated for different distances from aggregation center. The idea was to use the velocity information from groups of cells within each of the concentric rings. Arrows in the image show this idea: where the cAMP gradient is bigger then the mean of the velocities within that region will be higher from regions with a loss cAMP gradient. Distance between subsequent rings varied from 50 to 70 μm .

Results

Here are shown the quantitative results from tracking the movement of the fluorescent images from the merged frames during different stages of the multicellular developmental cycle. Cells trajectories are shown in Figure 4.1.

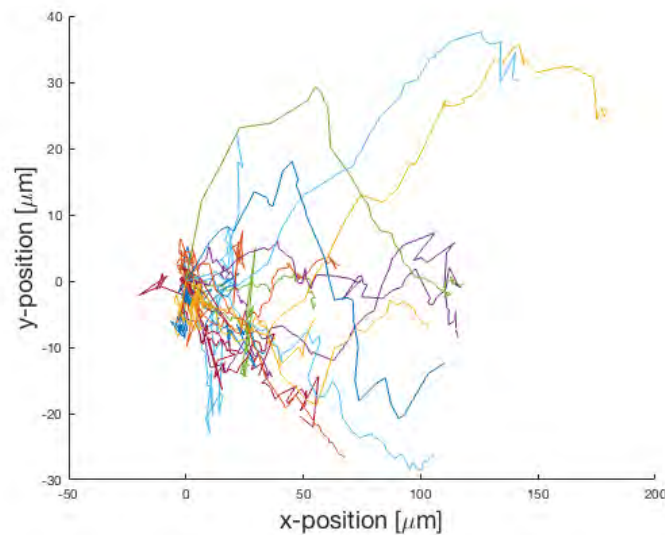


Figure 4.1: Individual trajectories from fluorescence observations with initial point translated to the x-y plane origin and rotated towards the relative direction of the aggregation center in the positive x-axis. Each color represents a different cell trajectory in a 50 minute time window after 2 hours of starvation.

TrackMate is an open ImageJ plug-in widely used for automatic and semi-automatic tracking (Tinevez et al. (2017)). Although this program can register

trajectories of cells very efficiently, it presented errors at the moment of implementation for the present study. First, it assigned false trajectories to cells due to the high cell density. This can be corrected manually but it would be time consuming because of the extensive amount of data. From here came the motivation for tracking a fraction of the total population which was labelled with fluorescent dyes. TrackMate also failed when tracking a smaller fraction because of bleaching. The program had errors to reassign a trajectory for cells that disappeared for some number of frames as was observed to happen. Figure 4.1 shows that these problems were solved by the algorithm pipeline written. The initial point of each trajectory was translated to the origin and all were rotated by the angle made between the first displacement and the aggregation center towards the positive x-axis, as the aggregation center lies in the (200,0) point. All cell trajectories plotted were a continuous curve and assignment of different cells to the same trajectory would be represented as discontinuous curves with an initial point not placed at the origin.

4.1 Time evolution

The time evolution of tracked *D. discoideum* cells is shown in Figure 4.2 for different time stages of aggregation in the same life cycle. The time step between subsequent frames is of one minute and the frame 51 in Figure 4.2 (a) was recorded approximately two hours after starving conditions were present. The segmenting, filtering and tracking process was performed in groups of 50 frames and the aggregation center is shown as a small circle with center in (2259,2400).

The Figure 4.2(a) shows short displacements over time with no apparent sense of direction. The panel (b) from the same figure shows longer displacements over time but still lacks of a general defined direction of motion for the next 50 minute window of observation, as seen in (a) of the same figure. Despite this, there are zones where some cells start to follow a direction of motion (as seen on the lower area from the aggregation center). The plot (c) shows the evolution of movement as the final aggregation, when the center appears. A clear directed motion towards this point with longer displacements was observed for this set of frames (Figure 4.2). Some cells were seen to follow a different direction but still with directed motion (upper left part). The final stages of aggregation are depicted in (d), where groups of cells are already co-localized in the aggregation center and other groups are still streaming towards the AgC.

Definition of the aggregation center could only be made manually. The problem faced is shown in Figure 4.3, where a group of cells started moving

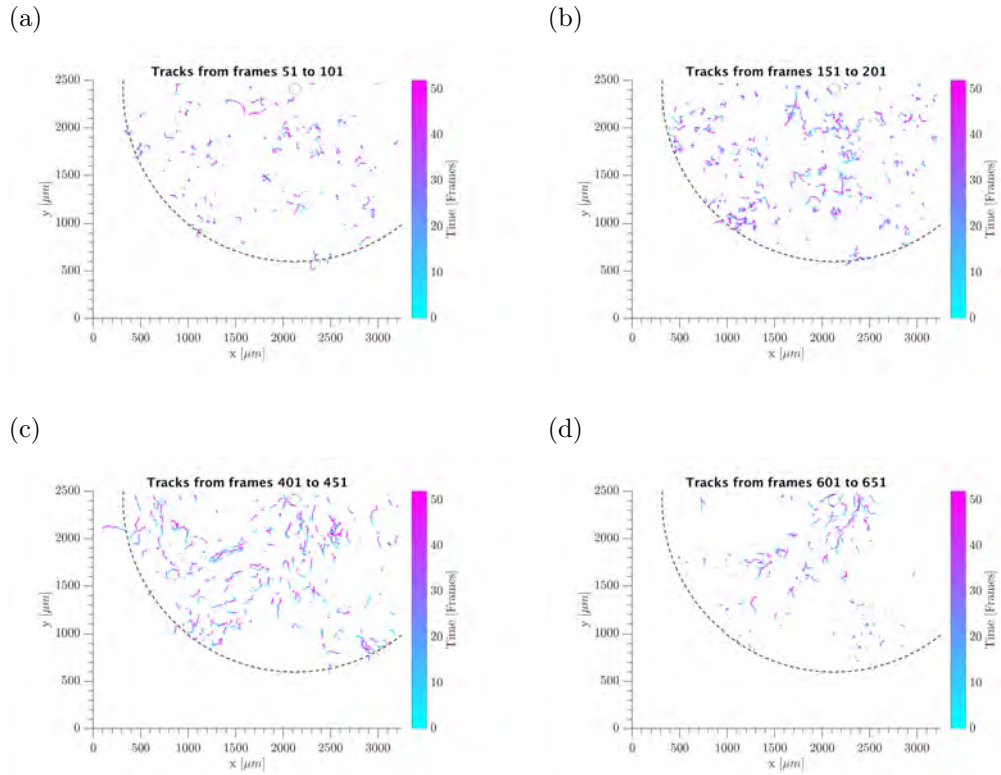


Figure 4.2: Surface plots of displacement's time evolution for red fluorescent stained cells. Experiment started after 1.5 hours of starving conditions, having frame 1 as the initial time. Each frame recording lasted 1 minute, so each figure shows the development of cells in a 50 minutes window time. (a) shows short tracks with no directed movement (2 hrs 20 min into life cycle like in Figure 1.1). (b) The cells have longer displacements but no directionality as well (4 hrs). (c) shows part of the aggregation stage with the cells moving towards the aggregation center (8 hrs 10 min). Streaming phase shown in (d) where cells merge together (11 hrs 30 min). The time reported in each frames set (figure) correspond to final time of the acquisition.

towards the right (Figure 4.3(a)) in what appeared to be the AgC. However, the directionality is lost at some point in time during the set frames from (b). Then the movement starts again in direction of the point in (2100,100) in (c) and at the end of the process two centers in close proximity can be distinguished from each other in panel (d). There is no explanation yet of why this happens and it is an open topic of research.

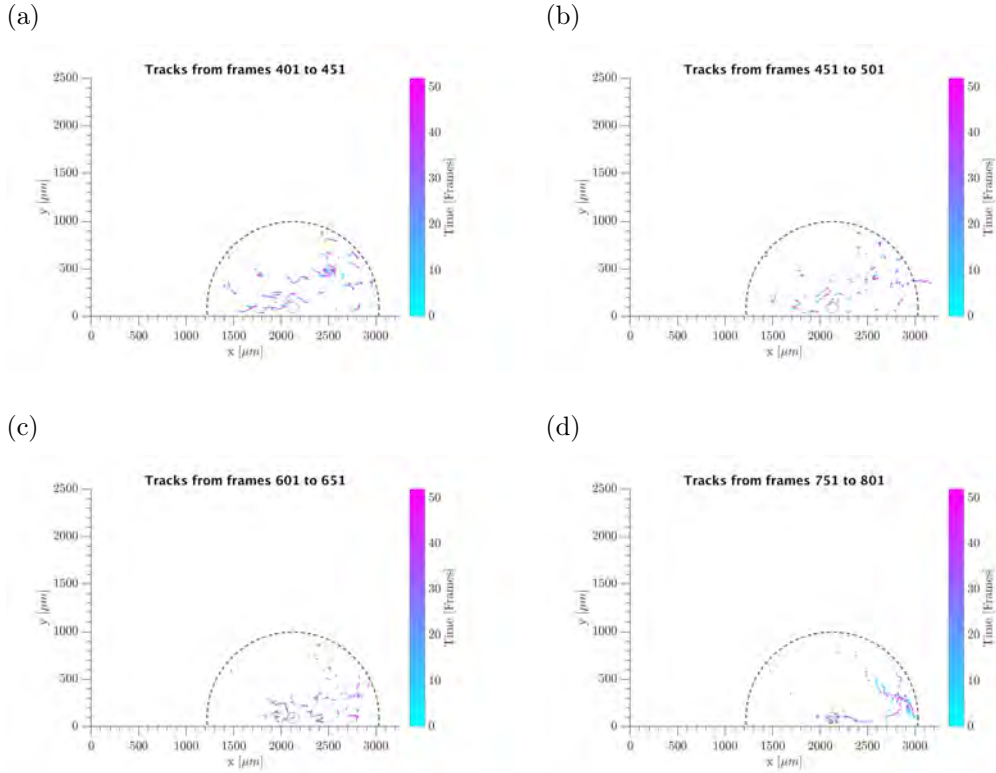


Figure 4.3: Problem faced for defining an AgC. Panel (a) shows directed motion towards a point which did not present an AgC in that location. The directionality is lost afterwards as shown in panel (b) and then recovered during the frames observed in panel (c). The last panel, (d), shows two apparent centers of aggregation in close proximity.

4.2 Chemotactic angle

The chemotactic angle (CA) evolution over time is shown in Figures 4.4 and 4.5 for the same experiment of last section.

Figure 4.4(a) shows the frames set before overall aggregation starts, with the CA distribution taking all values randomly. The corresponding histogram of the angle distribution is shown in (b) with the angle interval $[-180^\circ, 180^\circ]$ divided by 18 steps. The chemotactic angles had similar frequencies across all the values from the selected interval. Same distributions are shown in Figure 4.5 for a later time. Both the heat map and histogram show differences where the angle values become more frequent for numbers close to 0° , while the least frequent values were those close to 180° , corresponding to a directed movement away from the aggregation center. Negative values do not correspond to the same as their positive counterpart.

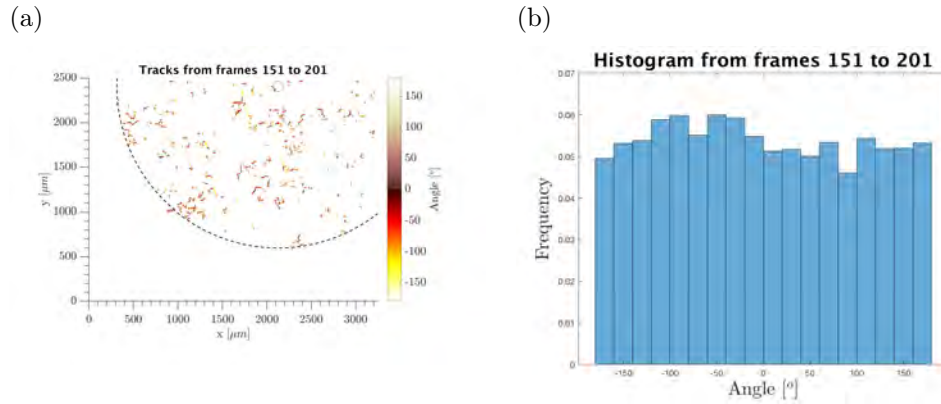


Figure 4.4: Time evolution of chemotactic angle for the same experiment type that was described in Figure 4.2. Random angle distribution is seen in (a) as a surface plot of the positions at a given time and more quantitatively in the corresponding histogram (b).

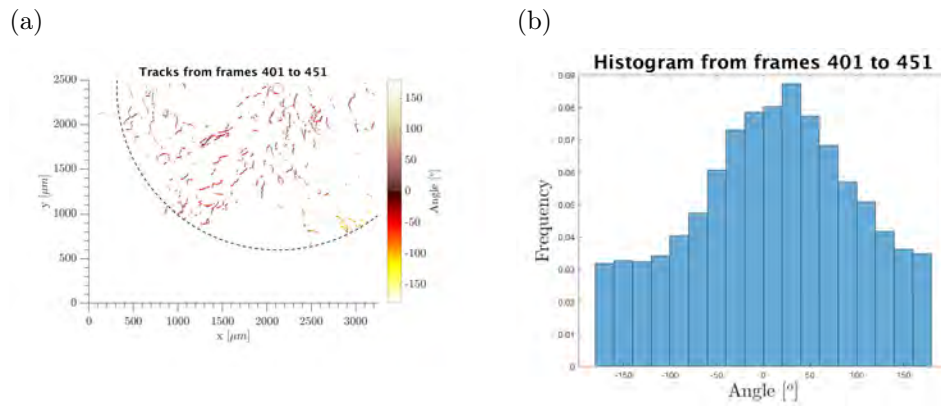


Figure 4.5: Time evolution of chemotactic angle as in Figure 4.4 but around 3 hours afterwards. The panel (a) shows the surface plot of chemotactic angles for each time displacement where values appear to be close to 0° . In (b) the angle histogram that shows quantitative directed motion of cells is present as the angle histogram is no longer randomly distributed.

Histograms like the one in Figure 4.5(b) were observed across different experiments where there was a clear AgC. On the other hand, no clear results could be obtained for cases like the one discussed in Figure 4.3. The underlying mechanism of how the final AgC is defined between two points close in space still needs to be addressed. One way of doing this could be by comparing histograms of multiple AgC with single ones. The angle distribution could point in a specific orientation above some threshold to know if cells around a circle will aggregate or not to a specific point.

4.3 Velocity

Velocities were also measured during different times of the life cycle. The respective surface plots and histograms of the same set of frames treated in previous sections can be seen in Figures 4.6 and 4.7. These values were obtained by dividing the spatial displacement with the time between those points. A measure of the velocity components with respect to the AgC was done as well. However, this appeared to give no useful information as the component heat maps and histograms looked the same. This represents a problem since a clear distribution was expected for the x-component of the velocities (the one pointing towards the AgC, see Figure 4.1). A reason for this behaviour could be that the time gap interval for the velocity calculation was taken too short, which does not allow to appreciate velocity changes over longer time intervals.

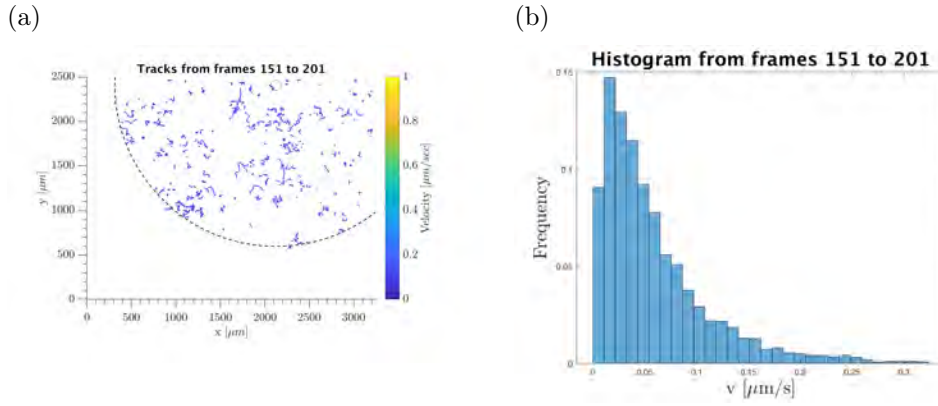


Figure 4.6: Evolution of cells speed with time. (a) Surface plot of velocity with respect to position for a 50 minute interval. (b) corresponding histogram.

The velocity histograms had no appreciable differences between them, unlike the angle distributions previously presented. The most frequent values were between 0.6-1.2 μ/min in both cases. Maximal speeds of 19.2 μ/min were recorded.

4.4 Passing waves

An estimation of cAMP relative concentration and gradient shape with respect to distance is shown in Figure 4.8 for different time gaps. Mean velocities are given in function of mean cells positions from AgC at each graph. Measurements were done for a 10 min time interval starting with the data obtained after 1.7 hours of no nutrient conditions (corresponding to frames 151-201 from

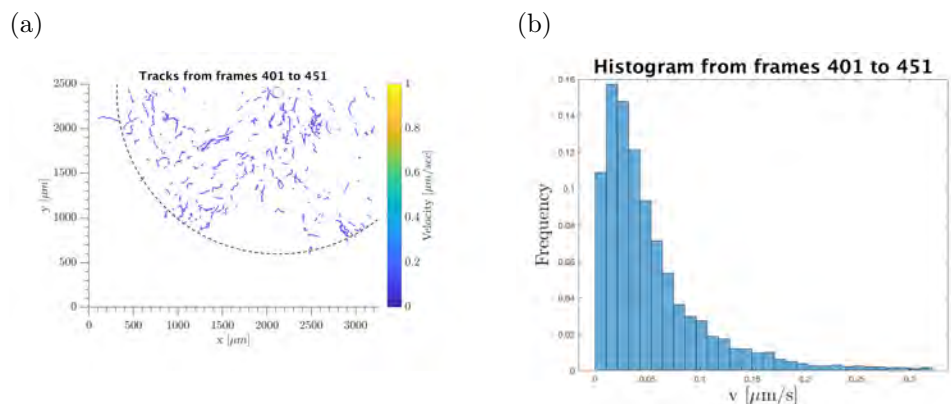


Figure 4.7: Evolution of cells speed with time. (a) Surface plot of velocity with respect to position for a 50 minute interval. (b) corresponding histogram.

previous sections). Although it is difficult to know the exact shape because of the error values, smooth periodic oscillations can be observed at some graphs like in (b), (c), and (f) of the Figure 4.8. These oscillations can not be visualized so easily at other time gaps like in (a), (d), and (e), although it could argue that some oscillatory behaviour is present.

Then it would be possible to determine the relative amount of chemoattractant molecules by analyzing the movement of cells. A maximum would be assigned to the greatest velocity. This would be a relative process with concentration values ranging from 0 to 1. Better values could be achieved by using longer time intervals to get better distributions of the velocities. It is important to note that other methods used to determine the cAMP gradient rely only on microscopy observations (Dormann et al. (2001), Ponsioen et al. (2004)). The velocity of the wave can be determined by dividing the distance between two maxima by one minute, which was the duration of each experiment shown in Figure 4.8. Wave values were in the range of 500 to 650 μm . A further approach could be to make a 2D color map showing the gradients shape by the relative concentration using the fact that it is possible to calculate the velocities.

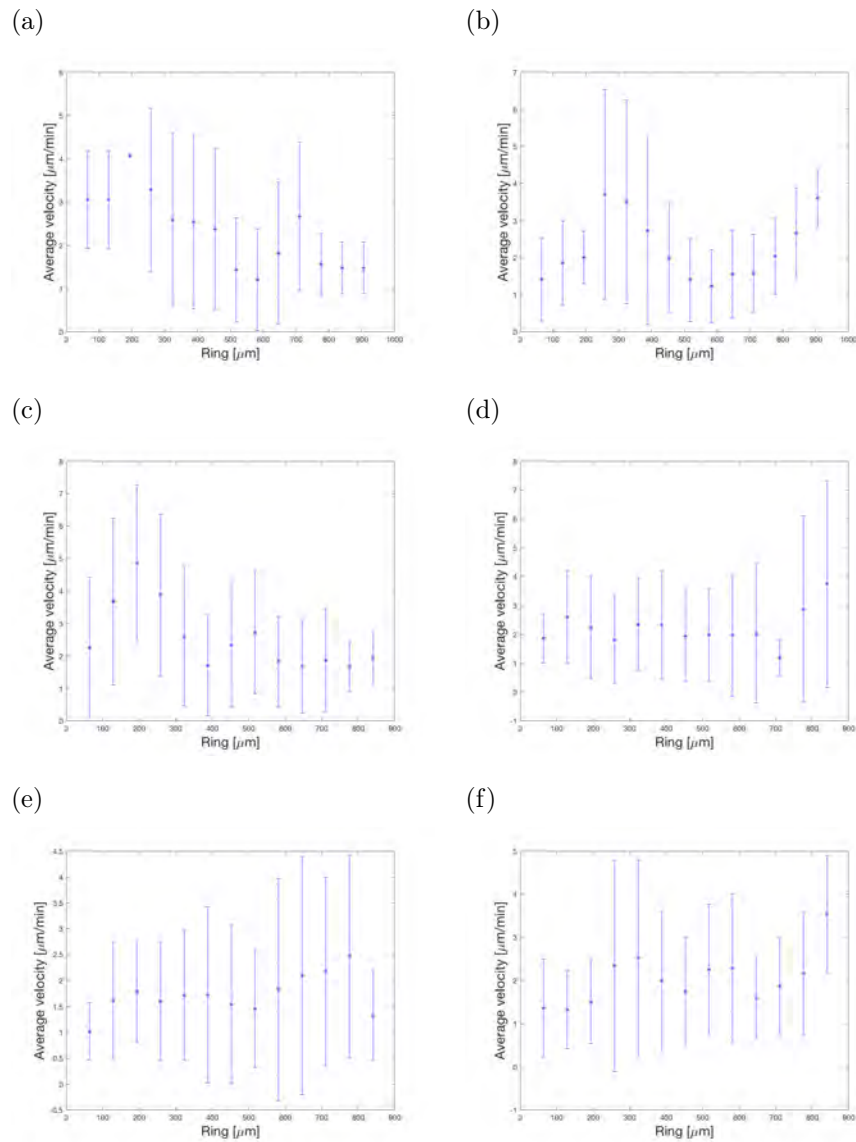


Figure 4.8: Velocity for cells within annular regions of 129.3 μm during a time gap of 10 minutes. Panel (a) contains the first set which started at 1.5 hours after starving conditions and there is a time gap of 1 hour between plots.

Conclusions

In summary, a method for studying multicellular aggregates was developed. Using an automated stage it was possible to visualize broader areas while having a 10X magnification. This method can be used for a broad variety of studies or to get data with higher statistics. As an example, it could improve similar experiments as in [McCann et al. \(2010\)](#) and [Wang et al. \(2014\)](#). Same observations and values were obtained for multiple experiments of multicellular aggregation, showing just two of the most representatives. Undoubtedly a bigger number of experiments would help improving the quality of data and the parameter values extracted.

Real-time imaging with both phase contrast and fluorescence microscopy allows this detection method to be quantitative. The time intervals and patterns observed fall in agreement with those known for *D. discoideum* life cycle [Kessin \(2001\)](#). A sequence of Matlab scripts were written so that they could be applied with relative ease for future studies of particle tracking. The randomness in (a) of Figure 4.2 could be explained by the early presence of cAMP gradients. Local aggregation centers come up in (b) from the same figure with local directed movement.

The histogram of (a) in Figure 4.4 shows no visible mean or shape and therefore represents a random variable. CA of collective migration is appreciated in (a) of Figure 4.5 where the color map has most of the values approaching to 0° . This can also be seen by the histogram in (d) where a mean over the 0° value is formed. This shows a directed motion of the displacement over a big number of the cells population. This also makes possible to identify quantitatively the exact point in time for aggregation.

Values up to $19.2 \mu\text{m}/\text{min}$ were observed and agree with previous estimations of *D. discoideum* speed, reported to be up to $20 \mu\text{m}/\text{min}$ ([Takagi et al. \(2008\)](#)). The velocity histograms were similar across different stages of the

life cycle, however, the earlier stage had a smaller count of values closer to $0.3\mu\text{m/s}$. This could be explained by the increase in velocity originated by a steeper cAMP gradients as the aggregation stage evolves. The similarity between histograms could be explained by different factors like the refraction period of the cells or the different cAMP wave shapes at unequal stages.

Movement of *D. discoideum* has been studied and reported for example in [Siegert et al. \(1994\)](#). However, the algorithms developed here can do a tracking of cells for longer periods of time and with a broader area of observation.

A possible method for calculation of relative cAMP gradients was proposed using the velocities measurements obtained and the fact that cell speed and cAMP gradients are directly related, as already mentioned in section 1.1.2 of the introduction from [Futrelle \(1982\)](#). This method consists on assigning the relative concentration value in function of the cells velocities. This was applied for gradients within concentric regions away from the aggregation center as depicted in [Figure 3.7](#). The wave velocities for these regions ranged from $500\mu\text{m}$ to $650\mu\text{m}$, which is in accordance with reported values of $600\mu\text{m}$ for initial stages of cAMP secretion [Rietdorf et al. \(1996\)](#). This method could lead to a new way to describe chemoattractant molecule gradients and concentrations without the necessity of using fluorescence microscopy ([Ponsioen et al. \(2004\)](#)) or darkfield methods([Dormann et al. \(2001\)](#)). A future project would be to change the algorithm in order to measure cAMP gradient and concentration by patched regions instead of concentric rings.

All the algorithms written are provided in the appendix section, they can be used with the proper citations.

Bibliography

- Abramowitz, M. and Davidson, M. W. Introduction to phase contrast.
- Amselem, G., Theves, M., Bae, A., Beta, C., and Bodenschatz, E. (2012a). Control parameter description of eukaryotic chemotaxis. *Physical review letters*, 109(10):108103.
- Amselem, G., Theves, M., Bae, A., Bodenschatz, E., and Beta, C. (2012b). A stochastic description of dictyostelium chemotaxis. *PloS one*, 7(5):e37213.
- Andrew, N. and Insall, R. H. (2007). Chemotaxis in shallow gradients is mediated independently of ptdins 3-kinase by biased choices between random protrusions. *Nature cell biology*, 9(2):193.
- Arthur, D. and Vassilvitskii, S. (2007). k-means++: The advantages of careful seeding. In *Proceedings of the eighteenth annual ACM-SIAM symposium on Discrete algorithms*, pages 1027–1035. Society for Industrial and Applied Mathematics.
- Baldauf, S. L. and Doolittle, W. F. (1997). Origin and evolution of the slime molds (mycetozoa). *Proceedings of the National Academy of Sciences*, 94(22):12007–12012.
- Blair and Dufresne (1997). The matlab particle tracking code repository. <http://physics.georgetown.edu/matlab/>. Accessed: 2018-06-30.
- Boedeker, H. U., Beta, C., Frank, T. D., and Bodenschatz, E. (2010). Quantitative analysis of random ameboid motion. *EPL (Europhysics Letters)*, 90(2):28005.
- Chan, T. F. and Shen, J. J. (2005). *Image processing and analysis: variational, PDE, wavelet, and stochastic methods*, volume 94. Siam.
- Chisholm, R. L. and Firtel, R. A. (2004). Insights into morphogenesis from a simple developmental system. *Nature reviews Molecular cell biology*, 5(7):531.

- Condeelis, J. and Segall, J. E. (2003). Intravital imaging of cell movement in tumours. *Nature Reviews Cancer*, 3(12):921.
- Crocker, J. C. and Grier, D. G. (1996). Methods of digital video microscopy for colloidal studies. *Journal of colloid and interface science*, 179(1):298–310.
- Cross, M. and Greenside, H. (2009). *Pattern formation and dynamics in nonequilibrium systems*. Cambridge University Press.
- Devreotes, P. N., Derstine, P. L., and Steck, T. L. (1979). Cyclic 3', 5'amp relay in dictyostelium discoideum. i. a technique to monitor responses to controlled stimuli. *The Journal of cell biology*, 80(2):291–299.
- Dormann, D., Kim, J.-Y., Devreotes, P. N., and Weijer, C. J. (2001). camp receptor affinity controls wave dynamics, geometry and morphogenesis in dictyostelium. *Journal of Cell Science*, 114(13):2513–2523.
- Edelstein, A. D., Tsuchida, M. A., Amodaj, N., Pinkard, H., Vale, R. D., and Stuurman, N. (2014). Advanced methods of microscope control using μ manager software. *Journal of biological methods*, 1(2).
- Eichinger, L., Pachebat, J., Glöckner, G., Rajandream, M.-A., Sucgang, R., Berriman, M., Song, J., Olsen, R., Szafranski, K., Xu, Q., et al. (2005). The genome of the social amoeba dictyostelium discoideum. *Nature*, 435(7038):43.
- Fey, P., Kowal, A. S., Gaudet, P., Pilcher, K. E., and Chisholm, R. L. (2007). Protocols for growth and development of dictyostelium discoideum. *Nature protocols*, 2(6):1307.
- Fisher, P. (1991). The role of gaseous metabolites in phototaxis by dictyostelium discoideum slugs. *FEMS microbiology letters*, 77(1):117–120.
- Friedrich, R., Siegert, S., Peinke, J., Siefert, M., Lindemann, M., Raethjen, J., Deuschl, G., Pfister, G., et al. (2000). Extracting model equations from experimental data. *Physics Letters A*, 271(3):217–222.
- Futrelle, R. (1982). Dictyostelium chemotactic response to spatial and temporal gradients. theories of the limits of chemotactic sensitivity and of pseudochemotaxis. *Journal of cellular biochemistry*, 18(2):197–212.
- Gerisch, G., Malchow, D., Roos, W., and Wick, U. (1979). Oscillations of cyclic nucleotide concentrations in relation to the excitability of dictyostelium cells. *Journal of Experimental Biology*, 81(1):33–47.

- Gholami, A., Steinbock, O., Zykov, V., and Bodenschatz, E. (2015). Flow-driven instabilities during pattern formation of dictyostelium discoideum. *New Journal of Physics*, 17(6):063007.
- Gonzalez, R. C., Woods, R. E., et al. (2002). *Digital image processing*. Prentice hall New Jersey.
- Haralick, R. M. and Shapiro, L. G. (1992). *Computer and robot vision*, volume 1. Addison-wesley Reading.
- Iranfar, N., Fuller, D., and Loomis, W. F. (2003). Genome-wide expression analyses of gene regulation during early development of dictyostelium discoideum. *Eukaryotic cell*, 2(4):664–670.
- Jensen, J. R. and Lulla, K. (1987). Introductory digital image processing: a remote sensing perspective.
- Jeon, K. (2012). *The biology of amoeba*. Elsevier.
- Kessin, R. H. (2001). *Dictyostelium: evolution, cell biology, and the development of multicellularity*, volume 38. Cambridge University Press.
- Lewis, J. P. (1995). Fast template matching. In *Vision interface*, volume 95, pages 15–19.
- Li, L., Nørrelykke, S. F., and Cox, E. C. (2008). Persistent cell motion in the absence of external signals: a search strategy for eukaryotic cells. *PLoS one*, 3(5):e2093.
- Lichtman, J. W. and Conchello, J.-A. (2005). Fluorescence microscopy. *Nature methods*, 2(12):910.
- McCann, C. P., Kriebel, P. W., Parent, C. A., and Losert, W. (2010). Cell speed, persistence and information transmission during signal relay and collective migration. *J Cell Sci*, 123(10):1724–1731.
- Negulescu, P. A., Krasieva, T. B., Khan, A., Kerschbaum, H. H., and Cahalan, M. D. (1996). Polarity of t cell shape, motility, and sensitivity to antigen. *Immunity*, 4(5):421–430.
- Nicol, A., Rappel, W., Levine, H., and Loomis, W. F. (1999). Cell-sorting in aggregates of dictyostelium discoideum. *J Cell Sci*, 112(22):3923–3929.
- O’Rourke, N. A., Dailey, M. E., Smith, S. J., and McConnell, S. K. (1992). Diverse migratory pathways in the developing cerebral cortex. *Science*, 258(5080):299–302.

- Parent, C. A. and Devreotes, P. N. (1999). A cell's sense of direction. *Science*, 284(5415):765–770.
- Ponsioen, B., Zhao, J., Riedl, J., Zwartkruis, F., van der Krogt, G., Zaccolo, M., Moolenaar, W. H., Bos, J. L., and Jalink, K. (2004). Detecting camp-induced epac activation by fluorescence resonance energy transfer: Epac as a novel camp indicator. *EMBO reports*, 5(12):1176–1180.
- Pupillo, M., Insall, R., Pitt, G. S., and Devreotes, P. N. (1992). Multiple cyclic amp receptors are linked to adenylyl cyclase in dictyostelium. *Molecular biology of the cell*, 3(11):1229–1234.
- Rietdorf, J., Siegert, F., and Weijer, C. J. (1996). Analysis of optical density wave propagation and cell movement during mound formation in dictyostelium discoideum. *Developmental biology*, 177(2):427–438.
- Saran, S., Meima, M. E., Alvarez-Curto, E., Weening, K. E., Rozen, D. E., and Schaap, P. (2002). camp signaling in dictyostelium. *Journal of Muscle Research & Cell Motility*, 23(7-8):793–802.
- Selmeczi, D., Mosler, S., Hagedorn, P. H., Larsen, N. B., and Flyvbjerg, H. (2005). Cell motility as persistent random motion: theories from experiments. *Biophysical journal*, 89(2):912–931.
- Shaffer, B. (1957). Aspects of aggregation in cellular slime moulds 1. orientation and chemotaxis. *The American Naturalist*, 91(856):19–35.
- Siegert, F., Weijer, C. J., Nomura, A., and Miike, H. (1994). A gradient method for the quantitative analysis of cell movement and tissue flow and its application to the analysis of multicellular dictyostelium development. *Journal of Cell Science*, 107(1):97–104.
- Siegert, S., Friedrich, R., and Peinke, J. (1998). Analysis of data sets of stochastic systems. *arXiv preprint cond-mat/9803250*.
- Song, L., Nadkarni, S. M., Bödeker, H. U., Beta, C., Bae, A., Franck, C., Rappel, W.-J., Loomis, W. F., and Bodenschatz, E. (2006). Dictyostelium discoideum chemotaxis: threshold for directed motion. *European journal of cell biology*, 85(9-10):981–989.
- Spath, H. (1985). *The cluster dissection and analysis theory fortran programs examples*. Prentice-Hall, Inc.
- Spence, M. T. and Johnson, I. D. (2010). *The molecular probes handbook: a guide to fluorescent probes and labeling technologies*. Live Technologies Corporation.

- Sussman, M. (1966). Biochemical and genetic methods in the study of cellular slime mold development1. In *Methods in Cell Biology*, volume 2, pages 397–410. Elsevier.
- Takagi, H., Sato, M. J., Yanagida, T., and Ueda, M. (2008). Functional analysis of spontaneous cell movement under different physiological conditions. *PLoS one*, 3(7):e2648.
- Tinevez, J.-Y., Perry, N., Schindelin, J., Hoopes, G. M., Reynolds, G. D., Laplantine, E., Bednarek, S. Y., Shorte, S. L., and Eliceiri, K. W. (2017). Trackmate: An open and extensible platform for single-particle tracking. *Methods*, 115:80–90.
- Tomchik, K. and Devreotes, P. (1981). Adenosine 3', 5'-monophosphate waves in dictyostelium discoideum: a demonstration by isotope dilution-fluorography. *Science*, 212(4493):443–446.
- Ungerer, F. and Schmid, H.-J. (2013). *An introduction to cognitive linguistics*. Routledge.
- Van Den Boomgaard, R. and Van Balen, R. (1992). Methods for fast morphological image transforms using bitmapped binary images. *CVGIP: Graphical Models and Image Processing*, 54(3):252–258.
- Van Haastert, P. J. and Devreotes, P. N. (2004). Chemotaxis: signalling the way forward. *Nature reviews Molecular cell biology*, 5(8):626.
- Varnum, B. and Soll, D. R. (1984). Effects of camp on single cell motility in dictyostelium. *The Journal of cell biology*, 99(3):1151–1155.
- Wang, C., Chowdhury, S., Driscoll, M., Parent, C. A., Gupta, S., and Losert, W. (2014). The interplay of cell–cell and cell–substrate adhesion in collective cell migration. *Journal of The Royal Society Interface*, 11(100):20140684.
- Watts, D. and Ashworth, J. (1970). Growth of myxamoebae of the cellular slime mould dictyostelium discoideum in axenic culture. *Biochemical Journal*, 119(2):171.
- Weijer, C. J. (1999). Morphogenetic cell movement in dictyostelium. In *Seminars in cell & developmental biology*, volume 10, pages 609–619. Elsevier.
- Weijer, C. J. (2004). Dictyostelium morphogenesis. *Current opinion in genetics & development*, 14(4):392–398.
- Weijer, C. J. (2009). Collective cell migration in development. *Journal of cell science*, 122(18):3215–3223.

Appendix A

Analysis list

```
1 %% Path information
2
3 path(path, '/Users/Desktop/Desired_folder/')
4
5 %% Assemble celltracker data sets
6
7 Assembly('2018-04-19', '002');
8 % Algorithm used to merge multiple frames.
9
10 % Images and alignment saved to specified folder.
11 %% Binarize celltracker data sets
12
13 Binarize_cellTracker('2018-04-19', 2, 250, 2, 3);
14
15 % Binarization made to identify actual cells from
    background.
16 %% Obtain tracks from binarized masks
17
18 obtainTracks('2018-05-30', 'ch3', 1, 401) % red
19
20 %% Calculate angle and velocity from the obtained tracks
21
22 datename = '2018-05-30'; % string
23 chName = 'ch3'; % string
24 least = 6; % integer
25 searchradius = 30; % integer (in px units)
```

```
26 center = ([3636 354]); % point (x,y) (in px units)
27 radius = 800; % integer (in px units)
28 scale = 100/154.67; %100 micrometers per 154.67 pixels.
29
30 vel_angle_extraction(datename, chName, least, searchradius,
    center, radius, scale)
31
32 %% Plot tracks
33
34 datename = '2018-05-30'; % string
35 chName = 'ch3'; % string
36 nr = 1; % Integer
37 plotfield = 'v_x'; % string, Possibilities: 'trackst', '
    v_x', 'v_y', 'velocity', 'angle_beta', 'angle_gamma', '
    angle_abs'
38
39 plot_tracks(datename, chName, nr, plotfield)
```

Appendix B

Assembly

```
1 function Assembly(datename)
2 %function Assembly(datename, expnr)
3
4 %expnr: experiment number
5
6 loadpath1 = [ '/Volumes/Sebi/' , datename , '/' , ];
7 % Folder from where to load data.
8
9 Dmax = dir([loadpath1 , '*.tif' ]);
10 ntot = str2double(Dmax(end).name(2:5));
11 nch = str2double(Dmax(end).name(8));
12
13 savepath_mat = [ '/Volumes/Sebi/' , datename , '_Testing' ];
14 % Folder to save path.
15
16 if exist(savepath_mat , 'dir') == 0
17     mkdir(savepath_mat)
18 end
19
20 Fsearch = 'F0001';
21 Smax = dir([loadpath1 , Fsearch , 'ch1_S*']);
22 Smax = numel(Smax); %Number of array elements.
23
24 switch Smax
25     case 16
26         Nrows = 4;
```

```

27     posrule = [1,2,3,4;...
28               8,7,6,5;...
29               9,10,11,12;...
30               16,15,14,13];
31 case 25
32     Nrows = 5;
33     posrule = [1,2,3,4,5;...
34               10,9,8,7,6;...
35               11,12,13,14,15;...
36               20,19,18,17,16;...
37               21,22,23,24,25];
38 end
39
40 cmat = dir([savepath_mat, '*ch*.mat']);
41
42 if isempty(cmat)
43
44     Alignvecx = zeros(size(posrule));
45     Alignvecy = zeros(size(posrule));
46
47     for a = 1:Nrows
48
49         Lvec = posrule(a,:);
50
51         for l = 2:length(Lvec)
52             D = dir([loadpath1, Fsearch, 'ch1_S', num2str(
53                   Lvec(l-1)), '_*']);
53             I1 = imread([loadpath1, D(1).name]);
54             D = dir([loadpath1, Fsearch, 'ch1_S', num2str(
55                   Lvec(l)), '_*']);
55             I2 = imread([loadpath1, D(1).name]);
56
57             pattern = I2(:,1:100);
58             Cx = normxcorr2(pattern, I1); %computes the
59                 normalized
59             %cross-correlation
60             %of the matrices template and A. The
61             %resulting matrix contains the
62             %correlation coefficients.
63
64             %To skip value
65             [~, imax] = max(abs(Cx(:)));

```

```

66         [ypeak, xpeak] = ind2sub(size(Cx),imax(1));
67         corr_offset = [(xpeak-size(pattern,2))
68                       (ypeak-size(pattern,1))];
69
70         xbegin = corr_offset(1) + 1;
71         ybegin = corr_offset(2) + 1;
72
73         Alignvecx(a,1) = xbegin;
74         Alignvecy(a,1) = ybegin;
75
76     end
77 end
78
79     Alignvecx = Alignvecx + 1;
80     Alignvecy = Alignvecy + 1;
81
82     Alignvecx = cumsum(Alignvecx,2);
83     Alignvecy = cumsum(Alignvecy,2);
84
85     Offsetx = zeros(Nrows-1,1);
86     Offsety = zeros(Nrows-1,1);
87
88     for a = 1:Nrows-1
89
90         if mod(a,2) == 1
91             L1 = posrule(a+1,end);
92             L2 = posrule(a,end);
93         else
94             L1 = posrule(a+1,1);
95             L2 = posrule(a,1);
96         end
97
98         D = dir([loadpath1, '*ch1_S', num2str(L1), '_*']);
99         I1 = imread([loadpath1,D(1).name]);
100        D = dir([loadpath1, '*ch1_S', num2str(L2), '_*']);
101        I2 = imread([loadpath1,D(1).name]);
102
103        pattern = I1(1:100,:);
104        Cx = normxcorr2(pattern,I2);
105
106        [~, imax] = max(abs(Cx(:)));
107        [ypeak, xpeak] = ind2sub(size(Cx),imax(1));

```



```

108     corr_offset = [(xpeak-size(pattern,2))
109                   (ypeak-size(pattern,1))];
110
111     sIm = size(I1);
112
113     xbegin = corr_offset(1) + 1;
114     ybegin = corr_offset(2) + 1;
115
116     Offsetx(a) = xbegin;
117     Offsety(a) = ybegin;
118 end
119
120 Offsetx = cumsum(Offsetx,1);
121 Offsety = cumsum(Offsety,1);
122
123 for a = 2:size(Alignvecx,1)
124     Alignvecx(a,:) = Alignvecx(a,:) + Offsetx(a-1);
125     Alignvecy(a,:) = Alignvecy(a,:) + Offsety(a-1);
126 end
127
128 if min(Alignvecx(:)) < 0
129     Alignvecx = Alignvecx + abs(min(Alignvecx(:))) +
130     1;
131 elseif min(Alignvecx(:)) == 0
132     Alignvecx = Alignvecx + 1;
133 end
134
135 if min(Alignvecy(:)) < 0
136     Alignvecy = Alignvecy + abs(min(Alignvecy(:))) +
137     1;
138 elseif min(Alignvecy(:)) == 0
139     Alignvecy = Alignvecy + 1;
140 end
141
142 else
143     M = load([savepath_mat, cmat(1).name]);
144
145     D = dir([loadpath1, '*ch1_S', num2str(1), '_*']);
146     I1 = imread([loadpath1, D(1).name]);
147
148     Alignvecx = M.Alignvecx;
149     Alignvecy = M.Alignvecy;

```

```

148 end
149
150 sim1 = max(Alignvecx(:)) + size(I1,2);
151 sim2 = max(Alignvecy(:)) + size(I1,1);
152
153 Fullmat = zeros(sim2, sim1);
154
155 for j = 1:nch
156     for i = 1:ntot
157
158         displaystring = [ 'Channel ', num2str(j), ' / ',
159                           num2str(nch), ' || Image ', num2str(i), ' / ',
160                           num2str(ntot) ];
161         disp(displaystring)
162
163         Fsearch = sprintf('%0.4d', i);
164         imgpath = [savepath_mat, 'ch', num2str(j), '/' ];
165
166         if exist(imgpath, 'dir') == 0
167             mkdir(imgpath)
168         end
169
170         imgname = [imgpath, sprintf('%0.4d', i), '.tif' ];
171
172         if exist(imgname, 'file') == 0
173
174             for a = 1:Nrows
175                 Lvec = posrule(a, :);
176                 for l = 1:length(Lvec)
177                     D = dir([loadpath1, 'F', Fsearch, 'ch',
178                             num2str(j), '_S', num2str(Lvec(l)),
179                             '_*' ]);
180                     if ~ isempty(D)
181                         I = imread([loadpath1, D(1).name
182                                     ]);
183                         xpos = [Alignvecx(a, l), Alignvecx
184                                 (a, l) + size(I, 2) - 1];
185                         ypos = [Alignvecy(a, l), Alignvecy
186                                 (a, l) + size(I, 1) - 1];
187                         Fullmat(ypos(1):ypos(2), xpos(1):
188                                 xpos(2)) = I;
189                     end
190                 end
191             end

```

```
182         end
183     end
184
185         imwrite( uint16(Fullmat),imgname, 'Compression
186             ', 'none')
187     end
188 end
189
190 savename = [savepath_mat, 'Alignement.mat'];
191 save(savename, 'Alignvecx', 'Alignvecy', 'sim1', 'sim2', '
192     datename')
```

Binarization

```
1 function Binarize_cellTracker(datename,chnr,initimg,kmin
   ,kmax)
2
3 % datename -> the folder name
4 % chnr -> Number of the channel to be evaluated (integer
   )
5 % initimg -> Number of the image, used for the initial
   threshold estimation
6 % kmin -> lower kmeans threshold (2-3)
7 % kmax -> upper kmeans threshold (mostly 3)
8
9 % Example:
10 % Binarize_cellTracker('2018-05-30',3,250,2,3);
11
12 loadpath1 = ['/Volumes/Sebi/',datename,'/ch',num2str(
   chnr),'/'];
13 % path used for previous function
14 savepath1 = ['/Volumes/Sebi/Mask/',datename,'/ch',
   num2str(chnr),'/'];
15 % desired path to save in specified folder
16
17 if exist(savepath1,'dir') == 0
18     mkdir
19         mkdir(savepath1)
20 end
21
```

```

22 D = dir([loadpath1, '*.tif']);
23
24 dbI = double(imread([loadpath1,D(initimg).name])); %
    apply kmeans clustering on the selected image
25 idx_in = find(dbI);%get rid of borders with no data
26 K_in = dbI(idx_in);
27
28 opts1 = statset('Display','off','UseParallel',1);
29 [~,C] = kmeans(double(K_in),2,'Replicates',4,'options',
    opts1);
30 Startset = C; % this is the statset to be used on all
    other frames
31 opts1 = statset('Display','off','UseParallel',0);
32
33 ntot = numel(D);
34
35 parfor i = 1:ntot % parallized the data analysis
36     savename = [savepath1,D(i).name];
37
38     if exist(savename,'file') == 0
39         displaystring = ['Binarizing image nr ',num2str
40             (i),' off ',num2str(ntot)];
41         disp(displaystring)
42
43         dbI = double(imread([loadpath1,D(i).name])); %
44             read frame
45         idx_in = find(dbI);
46         K_in = dbI(idx_in);
47
48         [ik,C] = kmeans(double(K_in),2,'Start',Startset
49             , 'options',opts1);
50         % apply kmeans, but this time not with a random
51             startpoint but the
52             % measured stats from the initial frame
53
54         [~,Fsort] = sort(C,'ascend');
55         idx = ismember(ik,Fsort(kmin:kmax));
56         % select the values to be part of the
57             binarization
58
59         BW = zeros(size(dbI));
60         BW(idx_in(idx)) = 1;

```

```
56     BW = BW > 0;
57     BW = bwareaopen(BW,10); % delete all objects
        smaller than 10 px
58
59     %st = strel('disk',2,0);%con 3?
60     st = strel('disk',4,0);
61     closeBW = imclose(BW,st);
62     BWf = imfill(closeBW,'holes');
63
64     imwrite(uint8(BWf)*255,savename)
65     end
66 end
```


Obtain Tracks

```
1 function obtainTracks(datename, chName, startframe ,
2     lastframe)
3 % Example:
4 % startframe = 1; % integer, first frame to be evaluated
5 % lastframe = 401; % integer, last frame to be evaluated
6 % datename = '2018-05-30'; % string
7 % chName = 'ch3'; % string
8 % obtainTracks(datename, chName, startframe, lastframe)
9
10 %%% of course other parameters like count (now ct) and
11 %%% the minimal and
12 %%% maximal size of the regarded regions could be a
13 %%% parameter parsed to
14 %%% the function
15
16 % Velocity and angle calculation for previously filtered
17 % masks.
18
19 loadpath1 = [ '/Volumes/Sebi/' , datename , chName , '/' ];
20 savepath1 = '/Volumes/Sebi/Tracks/';
21 D = dir([loadpath1, '*.tif']);
22 ct = 50;
23
24 %%% Initial frame is not necessary, rather a range in
25 %%% which the algorithm
```



```

22 %%% can be applied. So here a vector of numbers
    referencing the image
23 %%% ranges has to be evaluated
24
25 Fvec = startframe:ct:lastframe;
26 Tracklistcell = cell(length(Fvec),1); %%% this cell will
    collect all xys
27 %%% In the for loop 1 xys is created for each 50 frames
    between 1 and 401
28
29 Dnames = cell(numel(D),1); %%% the variable D will be
    sliced to use it in
30 % parallel processing
31
32 for d = 1:numel(Dnames)
33     Dnames{d} = [loadpath1 ,D(d).name];
34 end
35
36 for k = 1:length(Fvec)-1
37
38     imglist = Fvec(k):Fvec(k+1); %%% the list of images
        to be evaluated
39
40     %%% !!!! Attention: the parfor loop evaluates in
        parallel and therefore
41     %%% needs enough RAM. If this is not the case just
        exchange "parfor" by
42     %%% "for".
43
44     %%% The variables are sliced and collected in a cell
        during the
45     %%% independent parfor loops
46
47     cntcell = cell(length(imglist),1);
48     Subnames = Dnames(imglist);
49
50     %%% you can initialize the parallel pool by parpool(
        x), with x being
51     %%% the number of cores. But that obviously depends
        on the number of
52     %%% cores on your machine
53

```

```

54     %%% If you do not initialize it , then the computer
        will initialize it
55     %%% here with the default settings (can be changed
        under Preferences)
56
57     parfor i = 1:length(imglist)
58
59         displaystring = [ 'Evaluating image: ', num2str(
            imglist(i)), ' in segment k: ', num2str(k) ];
60         disp(displaystring)
61
62         BWf = imread(Subnames{i});
63         BWf_wo_s = bwareaopen(BWf,40);
64         R = regionprops(BWf_wo_s, 'Area');
65         F = find([R.Area]<200);
66         BW = ismember(bwlabel(BWf_wo_s),F);
67
68         BWbp = bpass(BW,1,31);
69         pk = pkfnd(BWbp,0.5,31);
70         cnt = cntrd(BWbp,pk,31);
71
72         cntcell{i} = cnt;
73     end
74
75     %%% the iterative way in which the celltracks are
        aligned , forbids
76     %%% usage in the parfor loop (in which the loops
        have to be independent)
77     %%% so the parfor loop covers the computationally
        intensive part and
78     %%% the rest is fast enough anyway
79
80     xys = [];
81
82     for i = 1:length(imglist)
83
84         cnt = cntcell{i}; %%% Unslicing of the variable
85
86         len = length(cnt);
87         z1 = ones(len,1);
88         z2 = [cnt(:,1) cnt(:,2) (z1+i)];
89         xys = [xys; z2];

```

```
90     end
91
92     Tracklistcell{k} = xys; %%% So Tracklistcell now
        collects xys for each
93                               %%% 50 frames long interval
94
95 end
96
97 savename = [savepath1 , datename , '_' , chName , '_tracks.mat'
98            ];
99 save(savename , 'Tracklistcell' , 'imglist' , 'Fvec' , 'Dnames')
```

Velocity and Angle Calculation

```
1 function vel_angle_extraction(datename, chName, least ,
    searchradius , center , radius , scale)
2
3 % Example
4
5 % datename = '2018-05-30'; % string
6 % chName = 'ch3'; % string
7 % least = 6; % integer
8 % searchradius = 30; % integer (in px units)
9 % center = ([3636 354]); % point (x,y) (in px units)
10 % radius = 800; % integer (in px units)
11 % scale = 100/154.67; %100 micrometers per 154.67 pixels
    .
12
13 % vel_angle_extraction(datename, chName, least ,
    searchradius , center , radius)
14
15 %%% Load matfile created by obtainTracks first
16
17 loadpath1 = '/Volumes/Sebi/Tracks/';
18 loadname = [loadpath1 , datename , '_' , chName , '_tracks.mat'
    ];
19 M = load(loadname);
20
21 %%% this one is now looped over all the xys obtained
    from the individual
```

```

22  %%% 50 frame long intervals
23
24  Trackevalcell = cell(size(M.Tracklistcell));
25
26  for mx = 1:size(M.Tracklistcell,1)
27
28      xys = M.Tracklistcell{mx};
29
30      if ~isempty(xys)
31
32          paramstr.mem = 0;
33          paramstr.quiet = 1;
34          paramstr.good = least;
35          paramstr.dim = length(xys(1,:))-1;
36
37          tracks = trackxys(xys,searchradius,paramstr);
38          tracksz = zeros(size(tracks,1),1);
39          %%% add a z (= 0) coordinate to use MATLAB's
          %%% pointcloud
40          ptCloud = pointCloud([tracks(:,1:2) tracksz]);
41          [idx,~] = findNeighborsInRadius(ptCloud,[center
          0],radius);
42          Fidx = unique(tracks(idx,4));
43          %%% finds all tracklabels which are within the
          %%% searchradius
44
45          [T,Tin] = annotate_tracks(tracks,Fidx,scale);
46          %%% check annotate_tracks on how to sort the
          %%% tracks
47          %%% T contains all tracks, Tin only the tracks
          %%% in the searchradius
48          %%% from here on all tracks are in micrometers
49          % add fieldnames to structure
50
51          field_names = {'tracksxmid','tracksymid','
          trackszmid','v_x','v_y','velocity','angle_abs
          ','angle_alpha','angle_beta','angle_gamma'};
52          empty_cells = repmat(cell(1),1,numel(field_names
          ));
53          entries = {field_names{:} ; empty_cells{:}};
54          s = struct(entries{:});
55          s = repmat(s,numel(Tin),1);

```

```
56     Tin = catstruct(Tin,s);
57
58     for t = 1:numel(Tin)
59         %%% run through all tracks within the radius
60
61         % Track to be evaluated
62
63         x = Tin(t).tracksx;
64         y = Tin(t).tracksy;
65
66         % middle point of trajectory
67         % (all later plotting values will be
68             assigned to this position)
69
70         xmid = (x(1:end-1)+x(2:end))/2;
71         ymid = (y(1:end-1)+y(2:end))/2;
72
73         % Velocity (calculated for each time step)
74
75         v_x = diff(x)./60;
76         v_y = diff(y)./60;
77         vel = (v_x.^2 + v_y.^2).^(1/2);
78         %%% the unit here is micrometer / second
79
80         %%% Started with the absolute angle and
81         %%% the relative angles for angle
82             calculation.
83
84         % absolute distance of each point from the
85             aggregation center
86
87         abs_dist = sqrt((center(1)-x).^2 + (center
88             (2)-y).^2);
89
90         % Absolute angle
91         %%% this the angle with respect to the
92             aggregation center
93         %%% it is calculated for each point and
94             together with the distance it would give
95         %%% the position of the cell in polar
96             coordinates
```

```

91     abs_angle = zeros(length(x),1);
92
93     for m = 1:length(x)
94
95         x2 = x(m) - center(1);
96         y2 = y(m) - center(2);
97         f = [x2,y2];
98         g = [1,0];
99
100        if f(2) < 0
101            ang = 360 - acosd(dot(f,g)/(norm(f)*
102                norm(g)));
103        elseif f(2) > 0
104            ang = acosd(dot(f,g)/(norm(f)*norm(g)
105                ));
106        else
107            if f(1) < 0
108                ang = 180;
109            else
110                ang = 0;
111            end
112        end
113
114        abs_angle(m) = ang;
115    end
116
117    % Relative angles (alpha, beta and gamma)
118    %%% alpha is +180 degrees to the abs_angle
119    (1)
120    %%% i.e. it is the absolute angle from the
121    first track segment to the aggregation
122    center
123
124    ang_alpha = wrapTo360(abs_angle(1) + 180); %
125    %%% circular quantity has to be wrapped
126    around
127
128    %%% beta is the angle between each
129    individual track segments
130    %%% gamma is the difference between alpha
131    and beta
132    %%% beta and gamma are vectors of length(x)

```

```

- 1
124
125     ang_beta = zeros(length(x)-1,1);
126
127     for m = 1:length(x)-1
128
129         a = x(m:m+1);
130         b = y(m:m+1);
131         x2 = a(2) - a(1);
132         y2 = b(2) - b(1);
133
134         f = [x2,y2];
135         g = [1,0];
136
137         if f(2) < 0
138             ang = 360 - acosd(dot(f,g)/(norm(f)*
139                               norm(g)));
139         elseif f(2) > 0
140             ang = acosd(dot(f,g)/(norm(f)*norm(g)
141                               ));
141         else
142             if f(1) < 0
143                 ang = 180;
144             else
145                 ang = 0;
146             end
147         end
148
149         ang_beta(m) = ang;
150     end
151
152     ang_gamma = wrapTo360(ang_alpha - ang_beta);
153
154     % fill structure
155
156     Tin(t).tracksxmid = xmid;
157     Tin(t).tracksymid = ymid;
158     Tin(t).trackszmid = zeros(1,length(xmid));
159     Tin(t).v_x = v_x;
160     Tin(t).v_y = v_y;
161     Tin(t).velocity = vel;
162     Tin(t).angle_abs = abs_angle;
```



```
163         Tin(t).angle_alpha = ang_alpha;
164         Tin(t).angle_beta = ang_beta;
165         Tin(t).angle_gamma = ang_gamma;
166
167     end
168
169     % Fill into cell
170
171     Trackevalcell{mx} = Tin;
172 end
173 end
174
175 % Read out size of image (will be only necessary for
    later plotting)
176
177 mask = imread(M.Dnames{1});
178 sizeimg = size(mask);
179 Fvec = M.Fvec;
180
181 savename = [loadpath1, datename, '_', chName, '_vel_ang.mat'
    ];
182 save(savename, 'Trackevalcell', 'center', 'radius', 'scale',
    'sizeimg', 'Fvec')
```